Supporting Information

Solvent-Dependent Transition from Concerted Electron-Proton to Proton Transfer in Photoinduced Reactions between Phenols and Polypyridine Ru Complexes with Proton-Accepting Sites

Sergei V. Lymar,* Mehmed Z. Ertem, and Dmitry E. Polyansky*
Chemistry Division, Brookhaven National Laboratory, Upton, New York 11973-5000, U.S.A.

Table of Contents

Section S1. Stern-Volmer Plots for Quenching of **X**(T) by *p*-Substituted Phenols.

All decay kinetics were exponential. The Stern-Volmer plots for quenching of **1**(T) by undeuterated *p*-substituted phenols in MeCN and CH_2Cl_2 appear in SI section S4 of our previous report.[1]

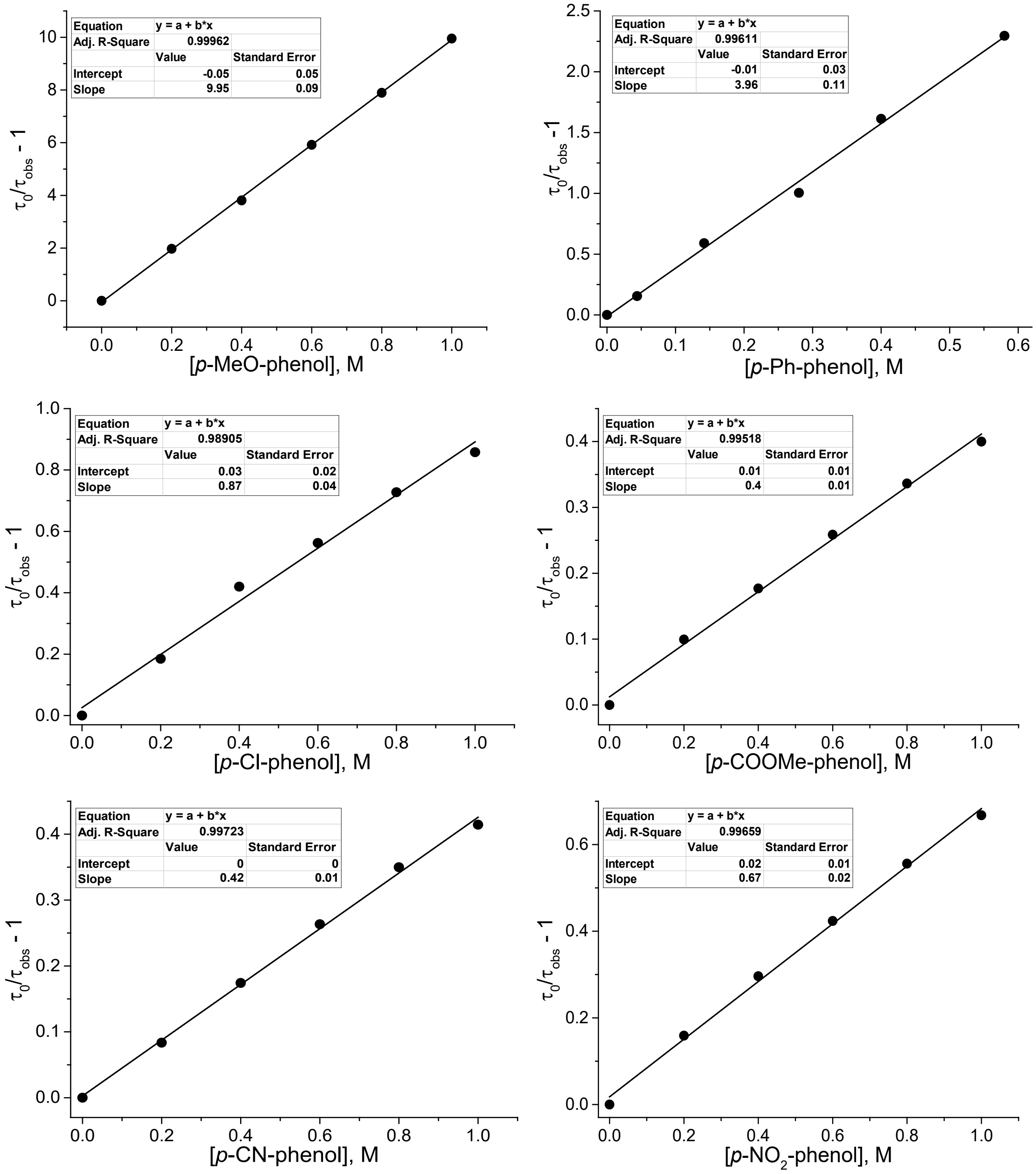

Equation	y = a + b*x	
Adj. R-Square	0.99962	
	Value	Standard Error
Intercept	-0.05	0.05
Slope	9.95	0.09

Equation	y = a + b*x	
Adj. R-Square	0.99611	
	Value	Standard Error
Intercept	-0.01	0.03
Slope	3.96	0.11

Equation	y = a + b*x	
Adj. R-Square	0.98905	
	Value	Standard Error
Intercept	0.03	0.02
Slope	0.87	0.04

Equation	y = a + b*x	
Adj. R-Square	0.99518	
	Value	Standard Error
Intercept	0.01	0.01
Slope	0.4	0.01

Equation	y = a + b*x	
Adj. R-Square	0.99723	
	Value	Standard Error
Intercept	0	0
Slope	0.42	0.01

Equation	y = a + b*x	
Adj. R-Square	0.99659	
	Value	Standard Error
Intercept	0.02	0.01
Slope	0.67	0.02

Figure S1.1. Stern-Volmer lifetime plots for quenching of **2**(T) by *p*-substituted phenols in MeCN (τ_0 = 430 ns). The maximum concentration of *p*-phenylphenol was limited by solubility.

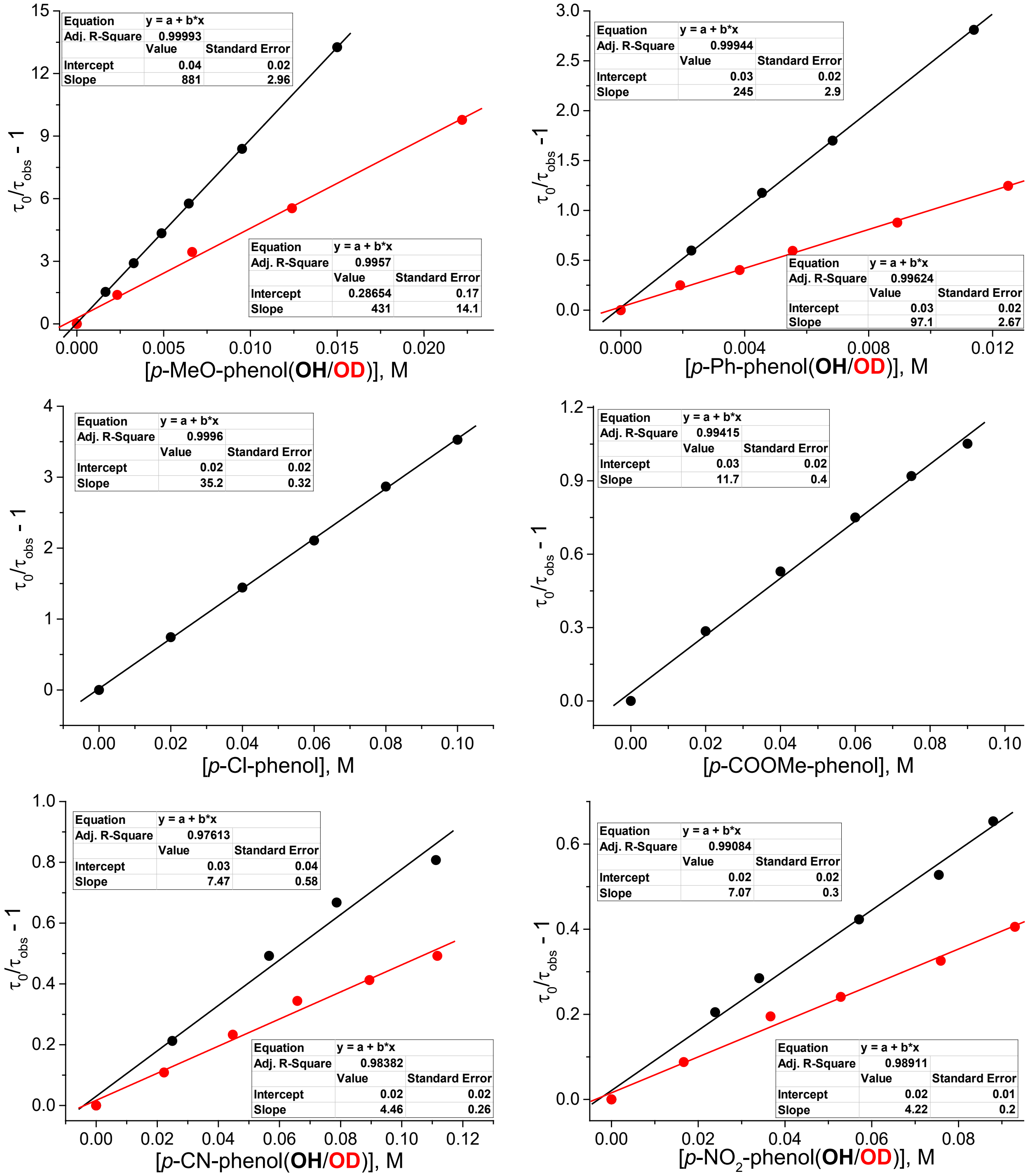

Figure S1.2. Stern-Volmer lifetime plots for quenching of **2**(T) by *p*-substituted phenols (O-H black; O-D red) in CH_2Cl_2 (τ_0 = 585 ns).

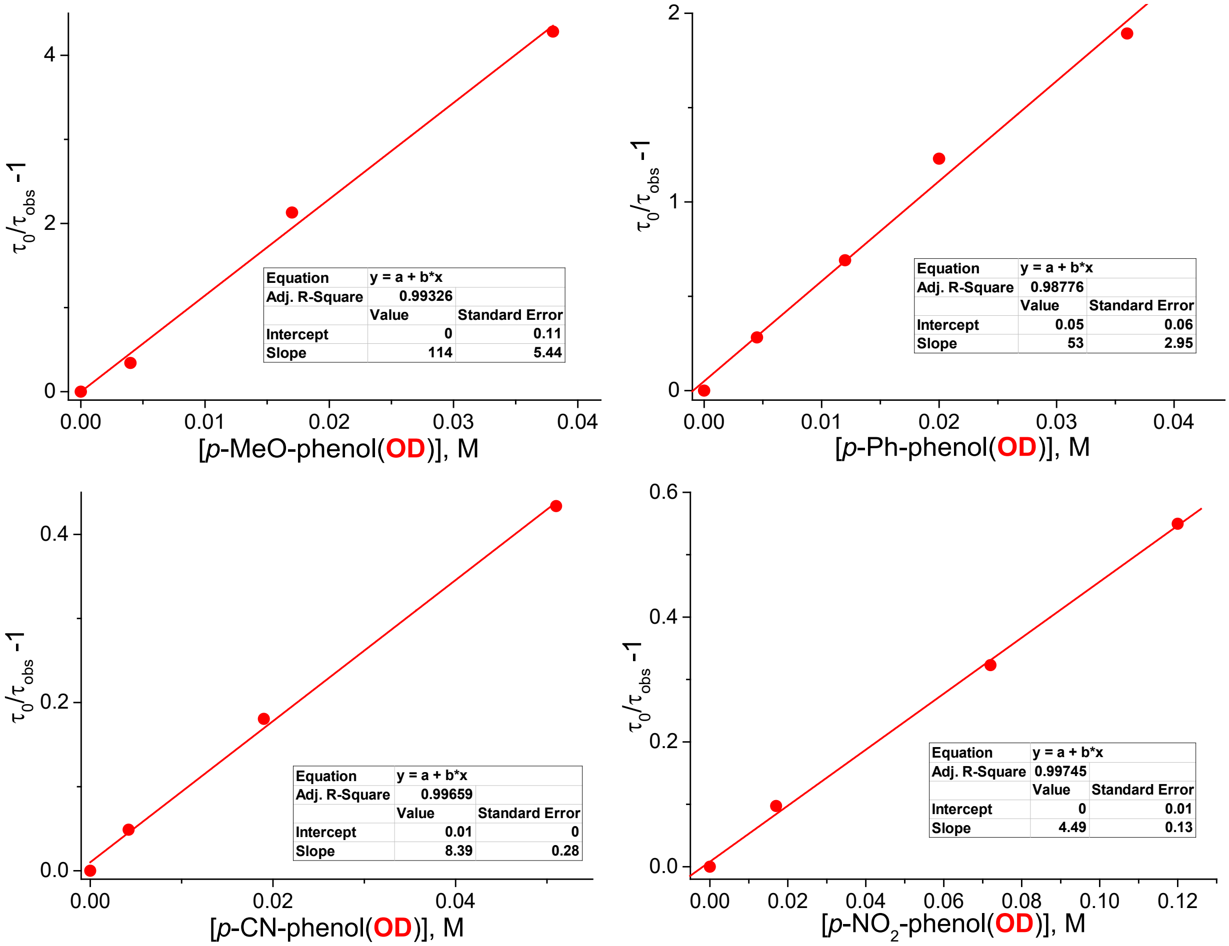

Equation	y = a + b*x	
Adj. R-Square	0.99326	
	Value	Standard Error
Intercept	0	0.11
Slope	114	5.44

Equation	y = a + b*x	
Adj. R-Square	0.98776	
	Value	Standard Error
Intercept	0.05	0.06
Slope	53	2.95

Equation	y = a + b*x	
Adj. R-Square	0.99659	
	Value	Standard Error
Intercept	0.01	0
Slope	8.39	0.28

Equation	y = a + b*x	
Adj. R-Square	0.99745	
	Value	Standard Error
Intercept	0	0.01
Slope	4.49	0.13

Figure S1.3. Stern-Volmer lifetime plots for quenching of **1**(T) by deuterated *p*-substituted phenols in CH_2Cl_2 (τ_0 = 350 ns).

Section S2. Gas-Phase and Solution Thermochemistry of Phenols, their Radical-Cations, and Phenoxyl Radicals.

I. Gas-phase O-H bond dissociation free energy ($BDFE_g$) in phenols.

These BDFE can be evaluated from the tabulated gas-phase O-H bond dissociation energies (BDE_g); that is,

$$BDFE_g = BDE_g + T[S^0(PhOH)_g - S^0(PhO^{\bullet})_g] - TS^0(H)_g \qquad (S2.1)$$

The gas-phase entropy difference between phenol and its radical should be small, nearly zero, and the gaseous H atom entropy is accurately known, $S^0(H)_g = 27.417$ cal/(mol K).[2] Thus,

$$BDFE_g \approx BDE_g - TS^0(H)_g \qquad (S2.2)$$

and BDFE calculated from this equation are included in Table 2 (main text) and Table S2.3.

II. Solvation free energy of phenol and phenoxyl radical.

The solution BDFE can be estimated from the gas phase values and free energies of gas-to-solvent transfers, that is,

$$BDFE_s = BDFE_g + [\Delta_{g\rightarrow s}G(PhO^{\bullet}) - \Delta_{g\rightarrow s}G(PhOH)] + \Delta_{g\rightarrow s}G(H) = BDFE_g + \Delta\Delta_{g\rightarrow s}G + \Delta_{g\rightarrow s}G(H) \qquad (S2.3)$$

where the subscript "s" indicates dissolved species, all (including H) in their standard states of 1 M ideal solution. To evaluate the $\Delta\Delta_{g\rightarrow s}G$ term, consider equilibria shown in the following scheme.

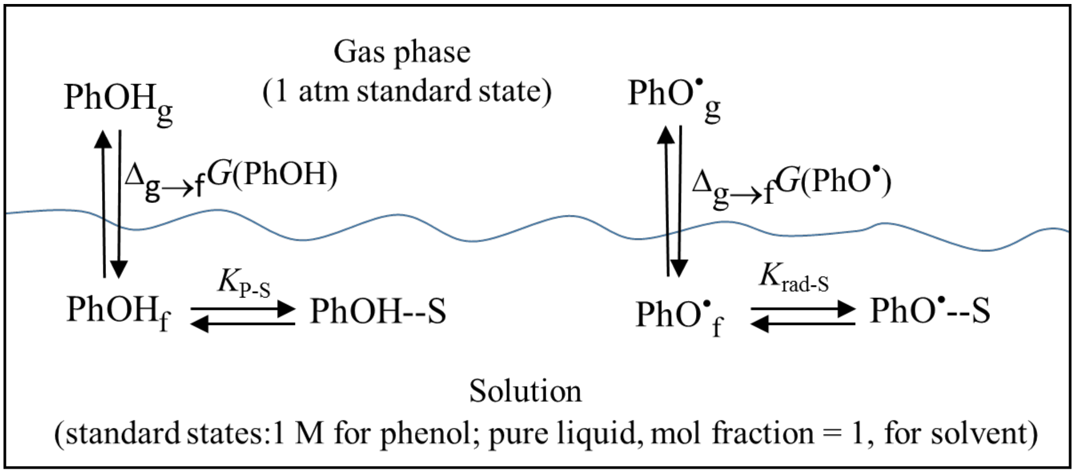

Here, $PhOH_f$ and $PhO^\bullet{}_f$ designate dissolved species that are "free" in the sense that they are not H-bonded to solvent. Thus, at equilibrium,

$$[\mathrm{PhOH_f}] = exp\left(-\Delta_{\mathrm{g}\to\mathrm{f}}G(\mathrm{PhOH})/RT\right) \tag{S2.4}$$

In the hydrogen bonding to solvent, phenol acts as an HB donor, and the distribution between the dissolved unbound and free phenol is described by,

$$K_{\text{P-S}} = [\text{PhOH--S}]/[\mathrm{PhOH_f}] \tag{S2.5}$$

From which the total phenol concentration in solution is,

$$[\mathrm{PhOH_s}] = [\mathrm{PhOH_f}] + [\text{PhOH--S}] = (1 + K_{\text{P-S}})[\mathrm{PhOH_f}] \tag{S2.6}$$

and the Henry's law constant (in M/atm) for phenol is given by,

$$K_{\mathrm{h}} = [\mathrm{PhOH_s}] = (1 + K_{\text{P-S}})[\mathrm{PhOH_f}] = exp\left(-\Delta_{\mathrm{g}\to\mathrm{s}}G(\mathrm{PhOH})/RT\right) \tag{S2.7}$$

Combining this equation with eq S2.4 we obtain,

$$\Delta_{\mathrm{g}\to\mathrm{s}}G(\mathrm{PhOH}) = -RTlnK_{\mathrm{h}} = \Delta_{\mathrm{g}\to\mathrm{f}}G(\mathrm{PhOH}) - RTln(1 + K_{\text{P-S}}) \tag{S2.8}$$

In contrast to the hydroxyl group of a phenol, the oxyl group of a phenoxyl radical acts as an HB acceptor toward the solvent, and the distribution between the unbound and bound $PhO^\bullet$ is given by,

$$K_{\text{rad-S}} = [\mathrm{PhO^\bullet}\text{--S}]/[\mathrm{PhO^\bullet{}_f}] \tag{S2.9}$$

Repeating the same derivations as in eqs S2.4-S2.8, we obtain,

$$\Delta_{\mathrm{g}\to\mathrm{s}}G(\mathrm{PhO^\bullet}) = \Delta_{\mathrm{g}\to\mathrm{f}}G(\mathrm{PhO^\bullet}) - RTln(1+K_{\text{rad-S}}) \tag{S2.10}$$

From eqs S2.8 and S2.10, the difference between the free energies of solvation of phenoxyl and phenol is,

$$\Delta\Delta_{\mathrm{g}\to\mathrm{s}}G = \Delta_{\mathrm{g}\to\mathrm{f}}G(\mathrm{PhO^\bullet}) - \Delta_{\mathrm{g}\to\mathrm{f}}G(\mathrm{PhOH}) + RTln\frac{1+K_{\text{P-S}}}{1+K_{\text{rad-S}}} \tag{S2.11}$$

Assuming that all interactions, except for the hydrogen bonding, between the solvent and phenol are the same as between the solvent and phenoxyl; that is,

$$\Delta_{\mathrm{g}\to\mathrm{f}}G(\mathrm{PhO^\bullet}) = \Delta_{\mathrm{g}\to\mathrm{f}}G(\mathrm{PhOH}) \tag{S2.12}$$

we can write,

$$\Delta\Delta_{\mathrm{g}\to\mathrm{s}}G = RTln\frac{1+K_{\text{P-S}}}{1+K_{\text{rad-S}}} \tag{S2.13}$$

The magnitudes of $K_{\text{P-S}}$ and $K_{\text{rad-S}}$ can be estimated using a well substantiated, empirical, thermodynamic scale for the 1:1 hydrogen bonding between uncharged species in CCl_4 developed by Abraham and co-workers,[3-5] according to which the HB strength is proportional to the HB acidity of the donor (α_2^{H}) and HB basicity of the acceptor (β_2^{H}). Applying the Abraham scale, taking into account solvent molar concentration, [S], and adopting the suggestion of Ingold and co-workers that for a given HB donor-acceptor pair the H-bonding constant is essentially independent of the surrounding medium,[6] we obtain for $K_{\text{P-S}}$,

$$logK_{\text{P-S}} = 7.354\alpha_2^{\mathrm{H}}(\mathrm{PhOH})\beta_2^{\mathrm{H}}(\mathrm{S}) + log[\mathrm{S}] - 1.094 \qquad \text{(S2.14)}$$

and for $K_{\text{rad-S}}$,

$$logK_{\text{rad-S}} = 7.354\beta_2^{\mathrm{H}}(\mathrm{PhO^\bullet})\alpha_2^{\mathrm{H}}(\mathrm{S}) + log[\mathrm{S}] - 1.094 \qquad \text{(S2.15)}$$

Table S2.1. Values of $K_{\text{P-S}}$ (eq S2.14), $K_{\text{rad-S}}$ (eq S2.16), and $\Delta\Delta_{\mathrm{g}\to\mathrm{s}}G$ (in kcal/mol, eq S2.13) for *p*-substituted phenols (R-PhOH) in three solvents. All values of α_2^{H} and β_2^{H} are taken from the work by Abraham and co-workers,[3-5] except for α_2^{H} of MeOC(O)-PhOH, which is derived from an interpolation in Figure S2.3.

R- (α_2^{H})	In MeCN α_2^{H} = 0.09; β_2^{H} = 0.44 $K_{\text{rad-S}} = 3.3$		In CH_2Cl_2 α_2^{H} = 0.13; β_2^{H} = 0.05 $K_{\text{rad-S}} = 3.9$		In H_2O α_2^{H} = 0.353; β_2^{H} = 0.38 $K_{\text{rad-S}} = 94$	
	$K_{\text{P-S}}$	$\Delta\Delta_{\mathrm{g}\to\mathrm{s}}G$	$K_{\text{P-S}}$	$\Delta\Delta_{\mathrm{g}\to\mathrm{s}}G$	$K_{\text{P-S}}$	$\Delta\Delta_{\mathrm{g}\to\mathrm{s}}G$
MeO- (0.573)	110	1.9	2.0	−0.28	180	0.38
Ph- (0.595)	130	2.0	2.1	−0.27	210	0.46
Cl- (0.670)	230	2.3	2.2	−0.24	330	0.74
MeOC(O)- (0.730)	350	2.6	2.3	−0.22	490	0.97
NC- (0.787)	540	2.9	2.4	−0.20	710	1.19
O_2N- (0.824)	710	3.0	2.5	−0.19	900	1.33

The values of α_2^{H} and β_2^{H} for phenols and solvents used in this work are known, which allows evaluating $K_{\text{P-S}}$ through eq S2.14, and the results are summarized in Table S2.2. Although β_2^{H} values for the PhO$^{\bullet}$ radicals are not known, Ingold and co-workers reasoned that the HB basicity of the oxyl in PhO$^{\bullet}$ can be well approximated by that of carbonyl.[7] We have chosen acetophenone (PhC(O)Me; $\alpha_2^{\mathrm{H}} = 0$, $\beta_2^{\mathrm{H}} = 0.51$)[5] as an H-bonding surrogate for all phenoxyl radicals, which yields,

$$log K_{\text{rad-S}} = 3.751\alpha_2^{\mathrm{H}}(\mathrm{S}) + log[\mathrm{S}] - 1.094 \qquad \text{(S2.16)}$$

The values of $K_{\text{rad-S}}$ obtained through this equation are also included in Table S2.2 along with the $\Delta\Delta_{\mathrm{g}\to\mathrm{s}}G$ values calculated from eq S2.13.

III. Relationship between solution BDFE, reduction potentials, and acid dissociation constants.

Several variations of the following thermochemical cycle involving a solute with a dissociable hydrogen atom, have been in use for a long time for connecting the A-H bond dissociation free energy in solution with acidities and reduction potentials

$$\begin{array}{rl}
\text{A-H}_{\mathrm{s}} = \mathrm{A_s}^{-} + \mathrm{H_s}^{+} & \Delta G = b\mathrm{p}K_{\mathrm{a}} \\
\mathrm{A_s}^{-} = \mathrm{A_s}^{\bullet} + \mathrm{e}^{-} & \Delta G = aE^{0}(\mathrm{A_s}^{\bullet/-}) \\
\mathrm{H_s}^{+} + \mathrm{e}^{-} = \tfrac{1}{2}\mathrm{H_2}(\text{ideal gas, 1 atm}) & \Delta G = -aE^{0}(\mathrm{H_s}^{+}/\tfrac{1}{2}\mathrm{H}_{2,\,\mathrm{g}}) \\
\tfrac{1}{2}\mathrm{H_2}(\text{ideal gas, 1 atm}) = \mathrm{H}(\text{ideal gas, 1 atm}) & \Delta G = \Delta_{\mathrm{f}}G(\mathrm{H_g}) \\
\mathrm{H}(\text{ideal gas, 1 atm}) = \mathrm{H_s} & \Delta G = \Delta_{\mathrm{g}\to\mathrm{s}}G(\mathrm{H}) \\
\hline
\text{Net:}\quad \text{A-H}_{\mathrm{s}} = \mathrm{A_s}^{\bullet} + \mathrm{H_s} & \Delta G = \mathrm{BDFE_s} \quad \text{(S2.17)}
\end{array}$$

Here, both half-cell reduction potentials are measured against the same reference electrode. Following Mayer and co-workers,[8] we have chosen the ferrocenium/ferrocene (Fc$^{+/0}$) half-cell in organic solvents and the standard hydrogen half-cell ($\mathrm{H_s}^{+}/\tfrac{1}{2}\mathrm{H}_{2,\,\mathrm{g}}$) in water. The coefficients a = 23.06 kcal/(mol V) and b = 1.364 kcal/mol serve to bring all ΔG values into the kcal/mol scale. From the scheme above it follows that,

$$\mathrm{BDFE_s} = aE^{0}(\mathrm{A_s}^{\bullet/-}) + b\mathrm{p}K_{\mathrm{a}} + \Delta_{\mathrm{f}}G(\mathrm{H_g}) + \Delta_{\mathrm{g}\to\mathrm{s}}G(\mathrm{H}) - aE^{0}(\mathrm{H_s}^{+}/\tfrac{1}{2}\mathrm{H}_{2,\,\mathrm{g}}) \qquad \text{(S2.18)}$$

or,

$$\mathrm{BDFE_s} = aE^{0}(\mathrm{A_s}^{\bullet/-}) + b\mathrm{p}K_{\mathrm{a}} + C_{\mathrm{G}} \qquad \text{(S2.19)}$$

where,

$$C_G = \Delta_f G(H_g) + \Delta_{g\rightarrow s}G(H) - aE^0(H_s^+/½H_{2,\,g}) \qquad (S2.20)$$

A similar cycle can be composed with the oxidized species, A-$H_s^{•+}$,

$$\begin{aligned}
\text{A-}H_s^{•+} &= A_s^{•} + H_s^{+} && \Delta G = bpK'_a\\
\text{A-}H_s &= \text{A-}H_s^{•+} + e^{-} && \Delta G = aE^0(AH_s^{•+/0})\\
H_s^{+} + e^{-} &= ½H_2(\text{ideal gas, 1 atm}) && \Delta G = -aE^0(H_s^+/½H_{2,\,g})\\
½H_2(\text{ideal gas, 1 atm}) &= H(\text{ideal gas, 1 atm}) && \Delta G = \Delta_f G(H_g)\\
H(\text{ideal gas, 1 atm}) &= H_s && \Delta G = \Delta_{g\rightarrow s}G(H)
\end{aligned}$$

$$\text{Net:}\quad \text{A-}H_s = A_s^{•} + H_s \qquad \Delta G = BDFE_s$$

This cycle yields,

$$BDFE_s = aE^0(AH_s^{•+/0}) + bpK'_a + C_G \qquad (S2.21)$$

Thus, eqs S2.19 and S2.21 can be combined to give,

$$BDFE_s = aE^0(A_s^{•/-}) + bpK_a + C_G = aE^0(AH_s^{•+/0}) + bpK'_a + C_G \qquad (S2.22)$$

The value of C_G in this equation depends on temperature, solvent, and the choices of reference electrode and standard states, but C_G is constant in the sense that it is independent of the chemical nature of A-H. The first term comprising C_G, namely the free energy of formation for gaseous H atom at 25 °C and 1 atm, provides the largest contribution and is accurately known $\Delta_f G(H_g)$ = 48.585 kcal/mol.[2] The other two terms are solvent-specific, and Table S2. gives their values along with C_G. Since no experimental data are available for the free energies of H solvation, a generally accepted assumption[8-10] is made here that $\Delta_{g\rightarrow s}G(H) = \Delta_{g\rightarrow s}G(H_2)$ for all solvents except water; a more accurate evaluation is available for the latter.[11]

There are non-trivial differences between our C_G values in Table S2. and their counterparts derived by Mayer and co-workers.[8] We feel that the importance of eq 2.22 due to its wide-spread use in the field warrants a brief comment. We note that Mayer and co-workers use the same assumption of $\Delta_{g\rightarrow s}G(H) = \Delta_{g\rightarrow s}G(H_2)$ and essentially the same data source for H_2 solubility in MeCN, but arrive at $\Delta_{g\rightarrow s}G(H_2)$ = 5.12 kcal/mol for MeCN, whereas our value that we use for calculating C_G is $\Delta_{g\rightarrow s}G(H_2)$ = 3.36 kcal/mol. Clearly, this discrepancy accounts for much of the disagreement in C_G for MeCN. It is easy to see that their $\Delta_{g\rightarrow s}G(H_2)$ value corresponds to

$\Delta_{g\to s}G(H_2) = -RTln(x)$ with $x = 1.8\times10^{-4}$ from Table S2., which would be correct for the standard state of dissolved H_2 defined as the mole fraction of unity. It is clear from Table S2. that the same situation exists with DMSO, DMF, and MeOH.

Table S2.2. Energetics of H_2 solvation and proton reduction in various solvents at 25 °C. Here, x is the mole fraction solubility of gaseous H_2 at 1 atm and K_h is the Henry's Law solubility constant $K_H = x$/(partial solvent molar volume). For all solvents, $\Delta_{g\to s}G(H_2)$ is calculated either as $\Delta_{g\to s}G(H_2) = -RTln(x)$ (if the standard state for dissolved H_2 is defined as a hypothetical $x = 1$ solution) or as $\Delta_{g\to s}G(H_2) = -RTln(K_h)$ (if the standard state for dissolved H_2 is defined as hypothetical 1 M solution). The latter value (for 1 M standard state) was substituted to eq S2.20 in place of $\Delta_{g\to s}G(H)$ to calculate C_G, *except* for water, where eq S2.23 was used.

Solvent	$10^4\times x$	$\Delta_{g\to s}G(H_2)$, kcal/mol $x = 1$ for $H_2(sol)$ st. state	$10^3\times K_h$, M/atm	$\Delta_{g\to s}G(H_2)$, kcal/mol 1 M for $H_2(sol)$ st. state	$E^0(H_s^+/½H_2)$, V vs $Fc^{+/0}$ (aE^0 kcal/mol)	C_G, kcal/mol (Warren et al.[8])
MeCN	1.80[12, 13]	5.11	3.42	3.36	−0.028[14] (−0.65)	**52.6** (54.9)
DMSO	0.76[15]	5.62	1.07	4.05	−0.732[16] (−16.88)	**69.5** (71.1)
DMF	1.47[12]	5.23	1.91	3.71	−0.69[16] (−15.91)	**68.2** (69.7)
MeOH	1.61[15]	5.17	2.09	3.66	−0.501[16] (−11.55)	**63.8** (65.3)
Solvent	$10^4\times x$	$\Delta_{g\to aq}G(H_2)$, kcal/mol $x = 1$ for $H_2(aq)$ st. state	$10^3\times K_h$, M/atm	$\Delta_{g\to aq}G(H_2)$, kcal/mol 1 M for $H_2(aq)$ st. state	$\Delta_{g\to aq}G(H)$, kcal/mol	C_G, kcal/mol (Warren et al.[8])
H_2O	0.1411[15]	6.62	0.781	4.24	4.78[11]	**53.4** (57.6)

A more natural choice of the electrochemical reference for $E^0(A_{aq}^{\bullet/-})$ or $E^0(AH_{aq}^{\bullet+/0})$ in aqueous solutions is the standard hydrogen electrode (SHE), so that $aE^0(H_{aq}^+/½H_{2,\,g}) = 0$ V by definition. Thus when $E^0(A_{aq}^{\bullet/-})$ or $E^0(AH_{aq}^{\bullet+/0})$ is measured against SHE, the C_G term for water becomes

$$C_G = \Delta_f G(H_g) + \Delta_{g\to aq}G(H) \qquad \text{(S2.23)}$$

Recently, the value of hydrogen atom hydration was critically evaluated to be $\Delta_{g\rightarrow aq}G(H) = 4.78 \pm 0.48$ kcal/mol.[11] Using this value, we obtain $C_G = 53.4$ kcal/mol for water. Thus, in aqueous solutions

$$\text{BDFE}_{aq}(\text{kcal/mol}) = aE^0(\text{A}_{aq}{}^{\bullet/-};\text{ SHE}) + b\text{p}K_a + 53.4 = aE^0(\text{AH}_{aq}{}^{\bullet+/0};\text{ SHE}) + b\text{p}K'_a + 53.4 \qquad \text{(S2.24)}$$

Our C_G value for water in Table S2. is about 4 kcal/mol lower than that recommended by Mayer and co-workers. We can only explain 1.8 kcal/mol of this difference by their use of $\Delta_{g\rightarrow aq}G(H_2)$ as a surrogate for $\Delta_{g\rightarrow aq}G(H)$ and the choice of standard state $x = 1$ for H_{aq}, but we have no explanation for the remaining discrepancy, save for a typo or arithmetic error.

Although the standard states are often a matter of choice, we do not believe that the choice of $x = 1$ only for the H_s standard state was deliberate by Mayer and co-workers because: (i) such a choice would definitely require explicit statement to this effect, (ii) it would be irrational, and (iii) it is impractical for the intended use of BDFE computed from eq S2.22, namely, evaluating the energetics of the H atom transfer from A-H in solution. Unfortunately, the use of incorrect C_G values impacts on a significant amount of the thermochemical data tabulated in the Mayer and co-workers' review;[8] substantial corrections may be in order.

IV. Thermochemistry of phenols, their radical-cations, and phenoxyl radicals in solution.

The thermochemical properties pertinent to the electron, proton, and H-atom transfers from phenols obtained using methodologies developed in subsections I-III above are collected in Table S2.3 below.

The solution BDFEs are estimated by combining eq S2.3 with S2.13, which gives,

$$\text{BDFE}_s = \text{BDFE}_g + RTln\frac{1+K_{\text{P-S}}}{1+K_{\text{rad-S}}} + \Delta_{g\rightarrow s}G(H) \qquad \text{(S2.25)}$$

and by using the data from Tables S2.1 and S2.2. Comparison of BDFE calculated using eq 2.24 from $\text{p}K_a(\text{PhOH})$ and $E^0(\text{PhO}^{\bullet/-})$ in water, the only solvent where these parameters have been measured, reveals a generally reasonable agreement with the solvation-based estimates through eq S2.25, which serves as a good justification of our use of the latter for deriving BDFE in MeCN and CH_2Cl_2.

Table S2.3. Thermochemistry at 25 °C of the O-H bond homolysis, Brønsted acidities (pK_a), and reduction potentials (E^0, V vs Fc$^{+/0}$ in MeCN and vs SHE in H_2O) of *p*-substituted phenols (R-PhOH). Also shown are the C_G values (from Table S2.) for water and acetonitrile and hydrogen bonding acidities (α_2^H) and basicities (β_2^H) derived by Abraham and co-workers.[3-5]

R- (α_2^H)	Gas phase		H_2O (C_G = 53.4 kcal/mol) α_2^H = 0.353; β_2^H = 0.38			MeCN (C_G = 52.6 kcal/mol) α_2^H = 0.09; β_2^H = 0.44				CH_2Cl_2 α_2^H = 0.13; β_2^H = 0.05
	BDE[a] kcal/mol	BDFE[b] kcal/mol	BDFE[c] kcal/mol	pK_a (PhOH)[17]	E^0 (PhO$^{•/–}$)[18]	BDFE[c] kcal/mol	pK_a (PhOH)	E^0 (PhO$^{•/–}$)[d]	E_p (PhOH$^{•+/0}$)[e]	BDFE[c] kcal/mol
MeO- (0.573)	84.2 ± 1.6	76.0	81.2 (79.7)	10.21	0.54	81.3	29.2[f]	–0.48	1.67	79.6
Ph- (0.595)	86.7 ± 1.7	78.5	83.8	9.55	na	83.9	27.2[f]	–0.25	1.86	82.1
Cl- (0.670)	90.7 ± 2.1	82.5	88.0 (84.6)	9.41	0.8	88.2	25.4[19]	0.04	2.23	86.1
NC- (0.787)	93.0 ± 1.8	84.8	90.8 (90.1)	7.97	1.12	91.1	22.7[20]	0.32	2.57	88.5
O_2N- (0.824)	93.9 ± 1.6	85.7	91.8 (91.2)	7.15	1.22	92.1	20.9[20]	0.48	2.74	89.4
H- (0.596)	86.7 ± 0.7	78.5	83.8 (85.2)	9.99	0.79	83.9	27.2[20]	–0.25	na	82.1

[a] For unsubstituted phenol, BDE is taken from a critical re-evaluation by Ingold and co-workers.[7] For all other phenols, multiple BDE entries in Luo's compilation[21] are averaged with the standard deviations shown; [b] Computed from eq S2.2 with $S^0(H)_g$ = 27.417 cal/(mol K);[2] [c] Estimated using eq S2.25. The values in parentheses are calculated using eq S2.24 from aqueous pK_a(PhOH) and E^0(PhO$^{•/–}$); [d] Derived using eq S2.22; [e] Irreversible CV peak potentials measured vs Ag/AgI;[22]; [f] Estimated from pK_a measurements in DMSO[22] and a well-behaved correlation for non-ortho-substituted phenols, pK_a(MeCN) = pK_a(DMSO) + (10.1±0.1).[20]

V. Hammett σ_p correlations of phenol's BDE, BDFE, potentials, and Brønsted and HB acidities.

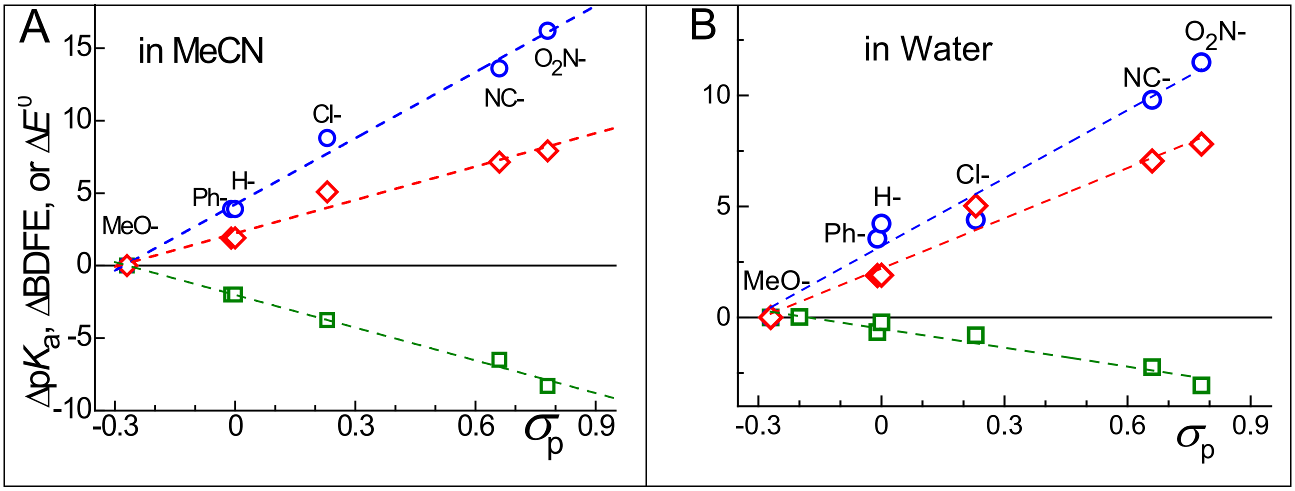

Figure S2.1. Hammett σ_p correlations for pK_a(PhOH) (green squares), BDFE (red diamonds), and $E^0(PhO^{\bullet/-})$ (blue circles) of *p*-substituted phenols in MeCN (A) and water (B) constructed from the data in Table S2.3. All quantities are relative to MeO-PhOH; that is, $\Delta pK_a(\text{R-PhOH}) = pK_a(\text{R-PhOH}) - pK_a(\text{MeO-PhOH})$. The BDFE (in kcal/mol) and E^0 (in V) values have been normalized to the same dimensionless decadic scale with pK_a; that is, ΔBDFE/1.364 and $\Delta E^0/0.059$ are plotted. The dashed lines show linear fits with the slopes absolute values in (A) $\rho = 7.5 \pm 0.4$ (bottom), 7.7 ± 0.7 (middle), and 15.2 ± 0.7 (top); (B) $\rho = 2.8 \pm 0.3$ (bottom), 7.5 ± 0.7 (middle), and 10.2 ± 0.7 (top).

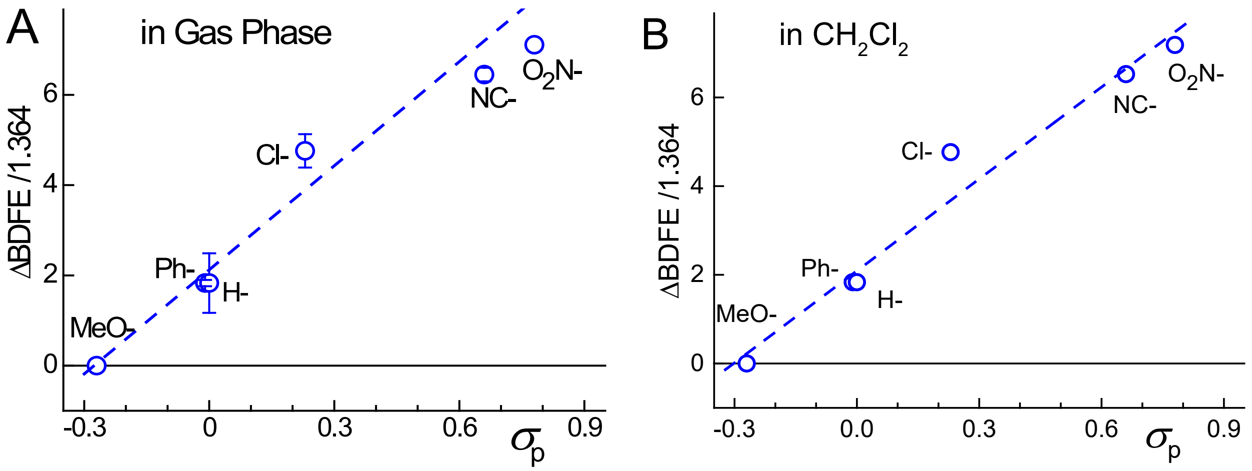

Figure S2.2. Hammett σ_p correlations of BDFE in gas-phase (A) and CH_2Cl_2 (B) for *p*-substituted phenols relative to MeO-PhOH (that is, ΔBDFE(R-PhOH) = BDFE(R-PhOH) – BDFE(MeO-PhOH)) constructed from the data in Table S2.3. The dashed lines show the linear fits with the slopes 6.8 ± 0.7 (A) and 6.9 ± 0.7 (B).

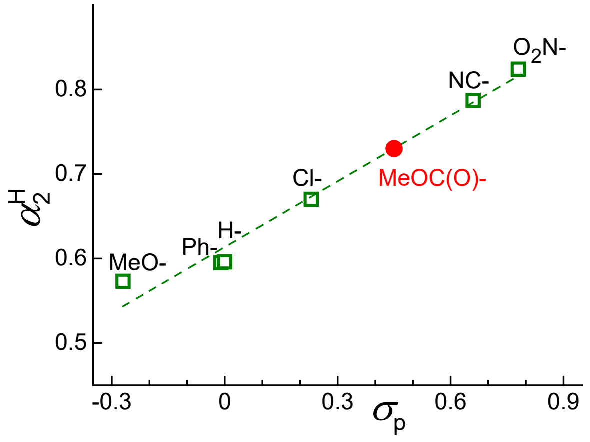

Figure S2.3. Hammett σ_p correlations of Abraham's HB acidity constant, α_2^H. The dashed line shows the linear fit with a slope of 0.26 ± 0.02 and intercept of 0.61 ± 0.01. These parameters along with $\sigma_p = 0.45$ for MeOC(O)-PhOH (Table 1, main text) have been used to estimate the previously unknown α_2^H of this phenol, which is shown as a red circle corresponding to α_2^H = 0.730.

Section S3. Thermochemical Results from Computational Studies.

The absolute free energies of *p*-substituted phenols (R-PhOH), their anions (R-PhO⁻), radical cations (R-PhOH$^{\bullet+}$), and phenoxyl radicals (R-PhO$^{\bullet}$) as well as those of complexes **1** and **2** in their ground (**X** and **X**-H^{+})), excited (**X**(T) and **X**(T)-H^{+}), and reduced (**X**$^{-}$ and **X**-H) states were computed at the M06 level of theory with the SMD continuum solvation model as detailed in the Computational methods (main text). These results were used to derive: (i) free energy changes for EPT, PT, and ET reactions (Table S3.1), (ii) relative O-H BDFE, acidities, and reduction potentials of phenols (Table S3.2), and (iii) relative N-H BDFE in **X**-H, acidities of **X**-H, **X**-H^{+}, and **X**(T)-H^{+}, and reduction potentials of **X**, **X**(T), and **X**(T)-H^{+} (Table S3.3)

I. EPT, PT, and ET pathways.

The computed standard free energy changes in the EPT, PT, and ET reactions for separated reactants and products (reactions 7-9 in the main text); that is,

$$\mathbf{X}(\mathrm{T}) + \mathrm{PhO\text{-}H} = \mathbf{X}\text{-}\mathrm{H} + \mathrm{PhO}^{\bullet} \qquad \Delta_{\mathrm{EPT}}G^{0}$$

$$\mathbf{X}(\mathrm{T}) + \mathrm{PhO\text{-}H} = \mathbf{X}(\mathrm{T})\text{-}\mathrm{H}^{+} + \mathrm{PhO}^{-} \qquad \Delta_{\mathrm{PT}}G^{0}$$

$$\mathbf{X}(\mathrm{T}) + \mathrm{PhO\text{-}H} = \mathbf{X}^{-} + \mathrm{PhO\text{-}H}^{\bullet+} \qquad \Delta_{\mathrm{ET}}G^{0}$$

are summarized in Table S3.1, and the values of $\Delta_{\mathrm{PT}}G^{0}$ and $\Delta_{\mathrm{ET}}G^{0}$ relative to $\Delta_{\mathrm{EPT}}G^{0}$ are plotted in Figure S3.1.

Table S3.1. Calculated $\Delta_{\mathrm{EPT}}G^0$, $\Delta_{\mathrm{PT}}G^0$, and $\Delta_{\mathrm{ET}}G^0$ (kcal/mol).

Substituent	X	in MeCN			in CH_2Cl_2		
		$\Delta_{\mathrm{EPT}}G^0$	$\Delta_{\mathrm{PT}}G^0$	$\Delta_{\mathrm{ET}}G^0$	$\Delta_{\mathrm{EPT}}G^0$	$\Delta_{\mathrm{PT}}G^0$	$\Delta_{\mathrm{ET}}G^0$
MeO-	**1**	−11.9	19.6	10.7	−14.0	35.4	6.1
	2	−8.5	26.2	8.6	−9.9	42.7	3.1
Ph-	**1**	−8.9	14.9	15.7	−10.9	30.6	11.2
	2	−5.5	21.5	13.6	−6.8	37.9	8.2
Cl-	**1**	−6.3	14.7	24.2	−8.5	30.0	20.2
	2	−2.9	21.3	22.1	−4.4	37.3	17.1
MeOC(O)-	**1**	−3.0	10.9	30.0	−5.2	26.1	26.2
	2	0.3	17.5	27.9	−1.1	33.4	23.2
NC-	**1**	−2.1	8.5	33.3	−4.4	23.2	29.8
	2	1.2	15.1	31.2	−0.3	30.5	26.8
O_2N-	**1**	−0.9	5.5	38.7	−2.9	19.9	34.7
	2	2.5	12.1	36.6	1.2	27.2	31.7

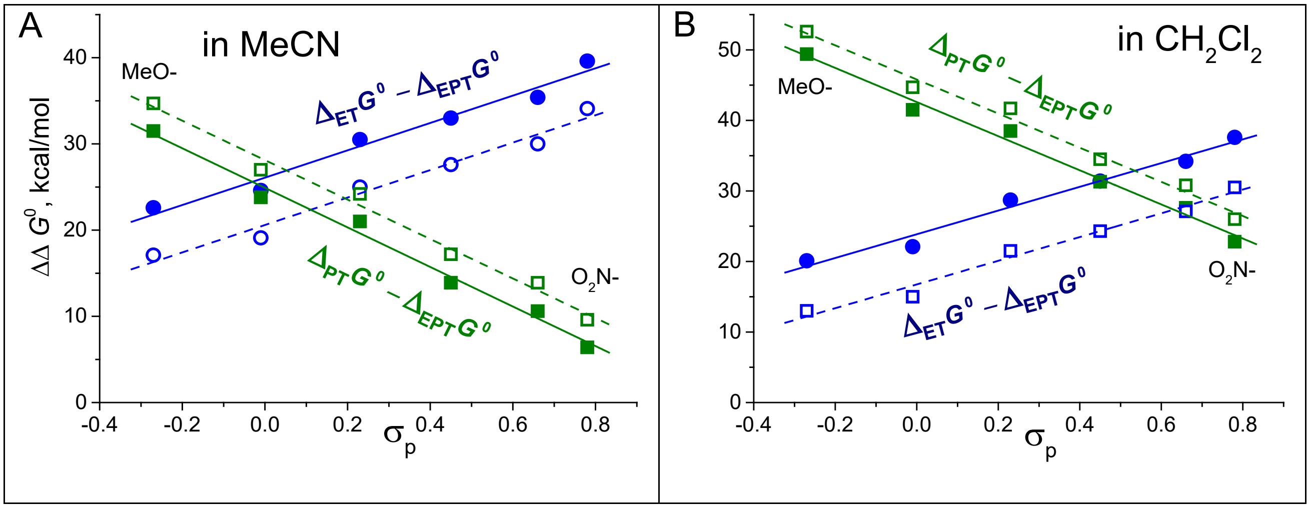

Figure S3.1. The σ_{p} dependencies of computed $\Delta\Delta G^0$ for PT (squares) and ET (circles) reactions relative to $\Delta_{\mathrm{EPT}}G^0$ ($\Delta\Delta G^0 = \Delta_{\mathrm{PT}}G^0 - \Delta_{\mathrm{EPT}}G^0$ and $\Delta\Delta G^0 = \Delta_{\mathrm{ET}}G^0 - \Delta_{\mathrm{EPT}}G^0$) between **1**(T) (solid symbols and lines) and **2**(T) (open symbols and dashed lines) and *p*-substituted phenols.

II. Phenols.

Various thermochemical parameters of *p*-substituted phenols relative to MeO-PhOH were computationally-evaluated. These quantities are collected in Table S3.2 and defined as follows:

R-PhO-H + MeO-PhO$^{\bullet}$ = R-PhO$^{\bullet}$ + MeOPhOH $\qquad \Delta G^0 = \Delta\mathrm{BDFE}$

MeO-PhOH + R-PhO^{-} = MeOPhO^{-} + R-PhOH $\qquad \Delta G^0 = b\Delta \mathrm{p}K_\mathrm{a}(\mathrm{PhOH})$

MeO-PhOH$^{\bullet+}$ + R-PhO$^{\bullet}$ = MeOPhO$^{\bullet}$ + R-PhOH$^{\bullet+}$ $\qquad \Delta G^0 = b\Delta \mathrm{p}K_\mathrm{a}(\mathrm{PhOH}^{\bullet+})$

MeO-PhO^{-} + R-PhO$^{\bullet}$ = MeOPhO$^{\bullet}$ + R-PhO^{-} $\qquad \Delta G^0 = a\Delta E^0(\mathrm{PhO}^{\bullet/-})$

MeO-PhOH + R-PhOH$^{\bullet+}$ = MeOPhOH$^{\bullet+}$ + R-PhOH $\qquad \Delta G^0 = a\Delta E^0(\mathrm{PhOH}^{\bullet+/0})$

where a = 23.06 kcal/(mol V) and b = 1.364 kcal/mol.

Table S3.2. Substituent effects on computed BDFE of the O-H bond (kcal/mol), Brønsted acidity, and reduction potential (V) of *p*-substituted phenols. The highlighted italicized values in parentheses are derived from the empirical estimates in Table S2.3 and shown for comparison.

R-	in MeCN					in CH_2Cl_2				
	ΔBDFE (PhO-H)	ΔpK_a (PhOH)	ΔE^0 (PhO$^{\bullet/-}$)	ΔpK_a (PhOH$^{\bullet+}$)	ΔE^0 (PhOH$^{\bullet+/0}$)	ΔBDFE (PhO-H)	ΔpK_a (PhOH)	ΔE^0 (PhO$^{\bullet/-}$)	ΔpK_a (PhOH$^{\bullet+}$)	ΔE^0 (PhOH$^{\bullet+/0}$)
MeO-	0	0	0	0	0	0	0	0	0	0
Ph-	3.0 *(2.6)*	−3.4 *(−2.0)*	0.33 *(0.23)*	−1.5	0.22 *(0.19)*	3.1 *(2.6)*	−3.5	0.34	−1.5	0.22
Cl-	5.6 *(6.9)*	−3.6 *(−3.8)*	0.46 *(0.52)*	−5.8	0.59 *(0.56)*	5.5 *(6.5)*	−4.0	0.47	−6.3	0.61
MeOC(O)-	8.9	−6.4	0.76	−7.6	0.84	8.8	−6.8	0.78	−8.3	0.87
NC-	9.8 *(9.7)*	−8.1 *(−6.5)*	0.91 *(0.80)*	−9.4	0.98 *(0.90)*	9.6 *(8.9)*	−8.9	0.95	−10.3	1.03
O_2N-	11.0 *(10.8)*	−10.3 *(−8.3)*	1.09 *(0.96)*	−12.5	1.21 *(1.07)*	11.1 *(9.8)*	−11.4	1.15	−12.8	1.24

Where available, comparison of computed and experiment-based estimates in this table shows an average disagreement within 0.7 kcal/mol for ΔBDFE, 1.3 units (1.8 kcal/mol) for ΔpK_a, and 85 mV (2.0 kcal/mol) for ΔE^0, which is comparable with the uncertainties of the empirical estimates themselves. Thus, we may expect our calculated relative $\Delta_{\mathrm{EPT}}G^0$, $\Delta_{\mathrm{PT}}G^0$, and $\Delta_{\mathrm{ET}}G^0$ for reactions of various phenols with the same **X**(T) to be, on the average, within ~2 kcal/mol of the actual values.

III. Ru complexes.

Various computationally-evaluated relative BDFE, reduction potentials, and pK$_a$ of complexes **1** and **2** as defined by the scheme below are summarized in Table S3.3.

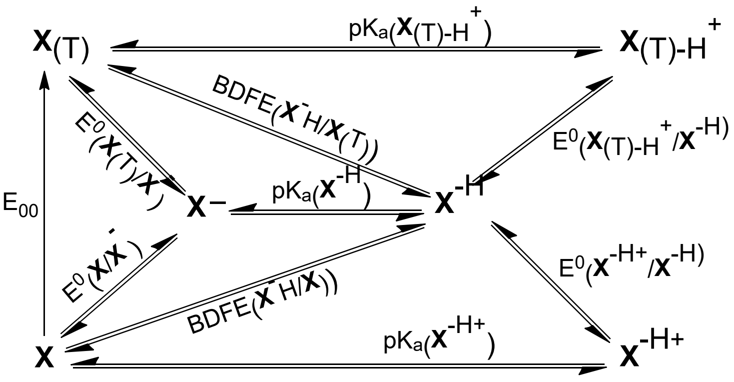

Table S3.3. Calculated relative triplet excitation energy (E_{00}), BDFEs of the N-H bond, reduction potentials, and Brønsted acidities of complexes **1** and **2**. The highlighted italicized values in parentheses are derived from the empirical estimates in Table S3.4 and shown for comparison.

Δ[quantity] = [quantity for **2**] – [quantity for **1**]	in MeCN	in CH_2Cl_2
ΔE_{00}, eV	0.25 (*exp. 0.30*)	0.30 (*exp. 0.3*)
ΔBDFE(**X**-H/**X**(T)), kcal/mol	–3.4	–4.1
ΔBDFE(**X**-H/**X**), kcal/mol	–9.1	–10
$\Delta E^0(\mathbf{X}(\mathrm{T})/\mathbf{X}^-)$, V	0.09 (*exp. 0.11*)	0.13
$\Delta E^0(\mathbf{X}/\mathbf{X}^-)$, V	–0.16 (*exp. –0.19*)	–0.13
$\Delta E^0(\mathbf{X}(\mathrm{T})\text{-H}^+/\mathbf{X}\text{-H})$, V	0.14	0.14
$\Delta E^0(\mathbf{X}\text{-H}^+/\mathbf{X}\text{-H})$, V	–0.01	–0.05
ΔpK$_a$(**X**-H)	–4.0	–5.2
ΔpK$_a$(**X**(T)-H$^+$)	–4.8	–5.4
ΔpK$_a$(**X**-H$^+$)	–6.5	–7.3

The computed and experiment-based estimates for ΔE_{00}, $\Delta E^0(\mathbf{X}(\mathrm{T})/\mathbf{X}^-)$, and $\Delta E^0(\mathbf{X}/\mathbf{X}^-)$ in this table shows an average disagreement on the order of 30 mV (0.7 kcal/mol), which is better than the uncertainties of the empirical values (~2 kcal/mol). Thus, we may expect our calculated relative $\Delta_{EPT}G^0$, $\Delta_{PT}G^0$, and $\Delta_{ET}G^0$ for reactions of the same phenol with **1**(T) and **2**(T) to be, on the average, within ~2 kcal/mol of actual values.

Table S3.4. Room temperature photophysical and redox properties of complexes **1** and **2** in MeCN and CH_2Cl_2.

Solvent	λ_{max} (abs.), nm[a]	λ_{max} (emis.), nm[b]	τ_0(T), ns[c]	$E_{1/2}(\mathbf{X}/\mathbf{X}^-)$, V[d, e]	E_{00}, eV[f]	$E^0(\mathbf{X}(\mathrm{T})/\mathbf{X}^-)$, V[d, g]
Complex **1**						
MeCN	528 ± 2	804 ± 5	190 ± 5	−1.10 ± 0.01[23]	1.7 ± 0.1	0.60 ± 0.11
CH_2Cl_2	525 ± 2	796 ± 5	350 ± 5	no data	1.7 ± 0.1	no data
Complex **2**						
MeCN	474 ± 2	680 ± 5	430 ± 5	−1.29 ± 0.01[24]	2.0 ± 0.1	0.71 ± 0.11
CH_2Cl_2	476 ± 2	671 ± 5	585 ± 5	no data	2.0 ± 0.1	no data
Complex **1i**						
MeCN	552	820	70	−1.13[23]	1.7 ± 0.1	0.57 ± 0.11
CH_2Cl_2	549	814	136	no data	1.7 ± 0.1	no data

[a] MLCT absorption band; [b] Triplet emission; [c] Triplet emission lifetime; [d] In V vs $Fc^{+/0}$ in MeCN; [e] Converted from values reported against SCE by subtracting 0.38 V;[25] [f] Energy difference between the lowest vibrational levels of the triplet and ground states estimated from the onset of triplet emission;[26] [g] Calculated from $E^0(\mathbf{X}(\mathrm{T})/\mathbf{X}^-) = E^0(\mathbf{X}/\mathbf{X}^-) + E_{00}$.

Table S3.5. Energetics of ion pairing between protonated Ru complexes X(T)-H$^+$ (actual charge $Z_X = +3$) and phenolates R-PhO$^-$ ($Z_P = -1$) and between reduced Ru complexes X$^-$ (actual charge $Z_X = +1$) and phenol radical cations R-PhOH$^+$ ($Z_P = +1$) The ion pairing equilibrium constants (K_{IP} in M^{-1}) and its associated free energy ($\Delta_{IP}G$ in kcal/mol) were evaluated using the expression suggested by Fuoss for spherical ions,[27]

$$K_{IP} = \frac{4\pi L r_0^3}{3000} exp\left(-\frac{W(r_0)}{kT}\right), \quad \text{where } W(r_0) = \frac{Z_X Z_P e^2}{D r_0}$$

Here, r_0 is the center-to-center separation of ions, *L* is the Avogadro number, *e* is the electron charge, *D* is the bulk dielectric constant of solvent, and the other symbols have their usual meanings. The value of r_0 can be roughly taken as the sum of the radii of equivalent spheres with volumes equal to the ions' volumes. The latter were computationally estimated as the volumes of solvent cavities created by ions upon their solvation. The average radii are: 5.0 ± 0.2 Å for complexes **1** and **2**, and 3.3 ± 0.1 Å for phenols.

Ion pair	Z_X	Z_P	in MeCN; D_{rel} = 35.94[28]		in CH_2Cl_2; D_{rel} = 8.93[28]	
			K_{IP}	$\Delta_{IP}G$	K_{IP}	$\Delta_{IP}G$
X(T)-H$^+$/PhO$^-$	+3	−1	4×10^2	−3.6	9×10^9	−13.6
X$^-$/PhOH$^{\bullet+}$	+1	+1	2×10^{-1}	0.9	8×10^{-4}	4.2

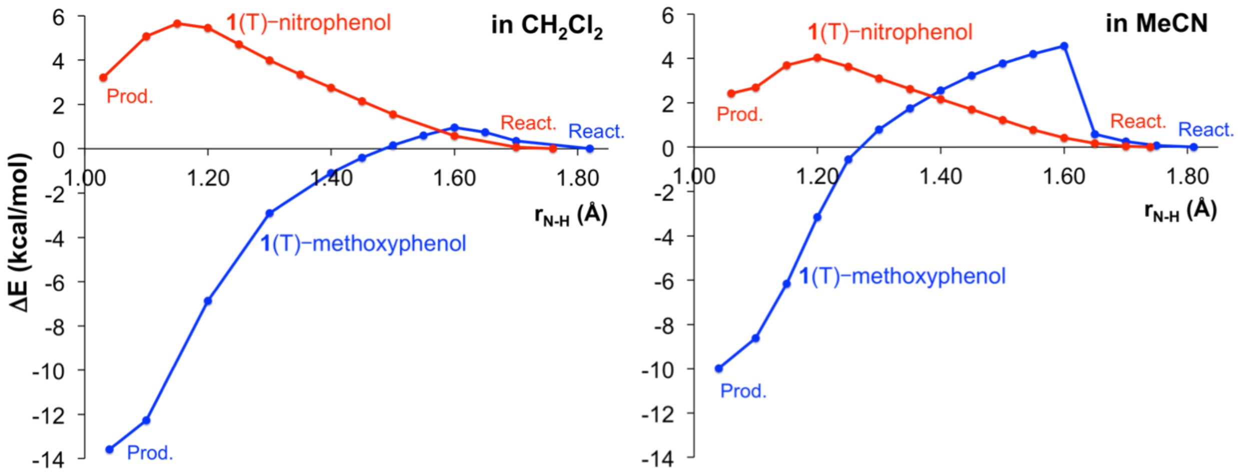

Figure S3.2. Energy profiles along the N-H distance between the ligand's quinoline N atom of **1**(T) and phenolic proton ($r_{\text{N-H}}$) in the **1**(T)-methoxyphenol and **1**(T)-nitrophenol H-bonded exciplexes in CH_2Cl_2 and MeCN obtained through a series of constrained geometry optimizations. The zero energy is assigned to the H-bonded reactant structures (React.) computed via unconstrained optimizations. Starting with these geometries, $r_{\text{N-H}}$ has been incrementally decreased by 0.05-0.10 Å, and the resulting structures were optimized to the lowest energy for each fixed $r_{\text{N-H}}$. The $r_{\text{N-H}}$ scanning continued until the product states (Prod.) were reached. The reactant and product structures with the unpaired spin density plots in Table S3.6 show that for **1**(T)-nitrophenol in MeCN the reaction products correspond to PT (that is, **1**(T)-H^+ and nitrophenoxide anion), whereas in all other cases the reaction products are those due to EPT (that is, **1**-H and phenoxyl radical).

Table S3.6. Computed structures with the unpaired spin density corresponding to the reactant and product states in Figure S3.2.

<table>
<tr><th colspan="2">in CH_2Cl_2</th></tr>
<tr><td>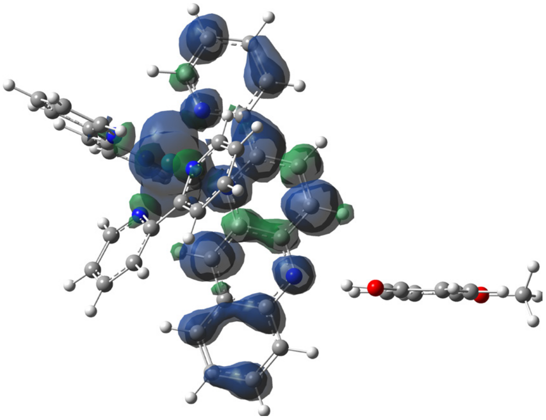
Reactant: **1**(T) – MeOPhOH</td><td>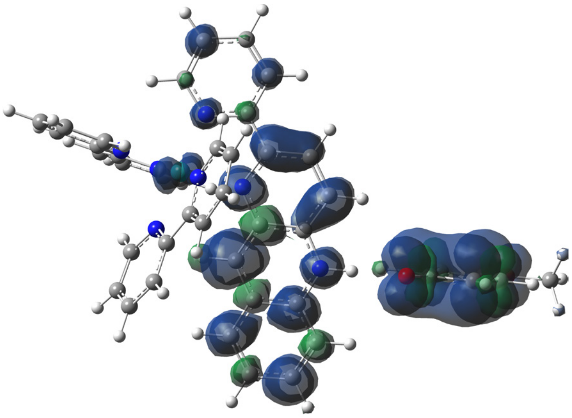
Product: (**1**-H) – MeOPhO$^\bullet$</td></tr>
<tr><td>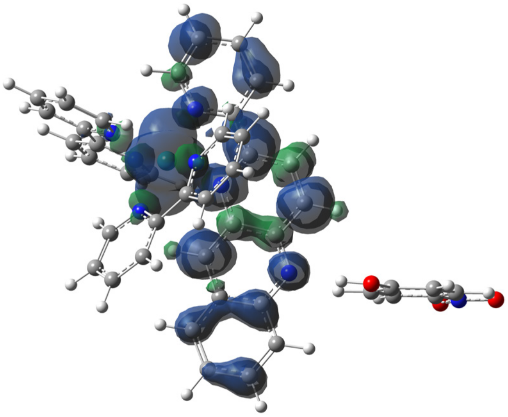
Reactant: **1**(T)–O_2NPhOH</td><td>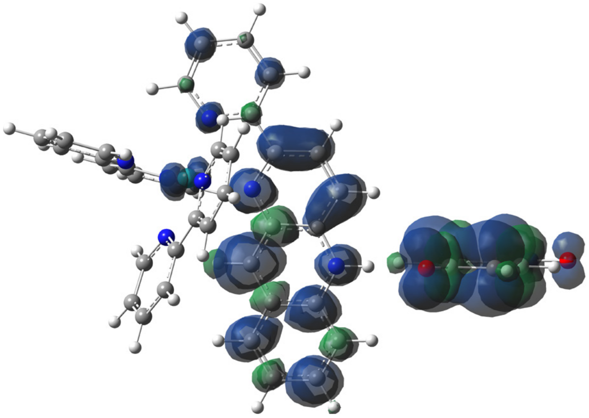
Product: **1**-H–O_2NPhO$^\bullet$</td></tr>
</table>

Table S3.6 (continued)

in MeCN	
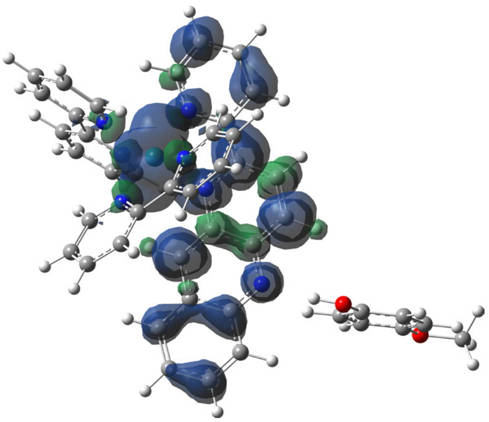 Reactant: **1**(T)–MeOPhOH	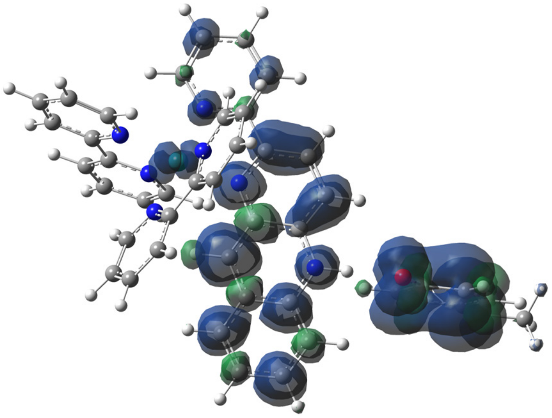 Product: **1**-H–MeOPhO$^\bullet$
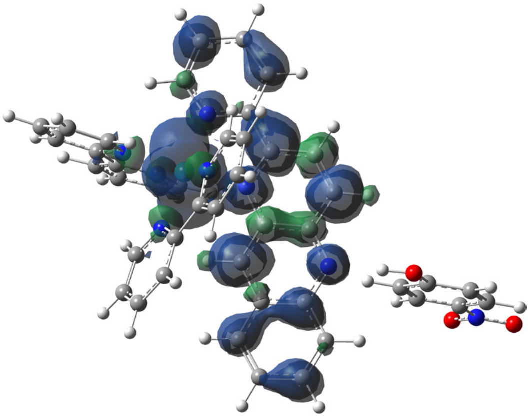 Reactant: **1**(T)–O_2NPhOH	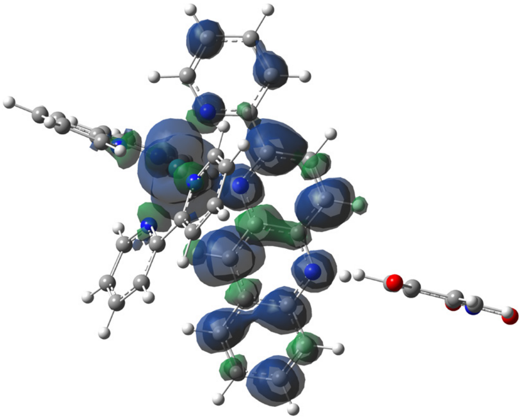 Product: **1**(T)-H$^+$–O_2NPhO$^-$

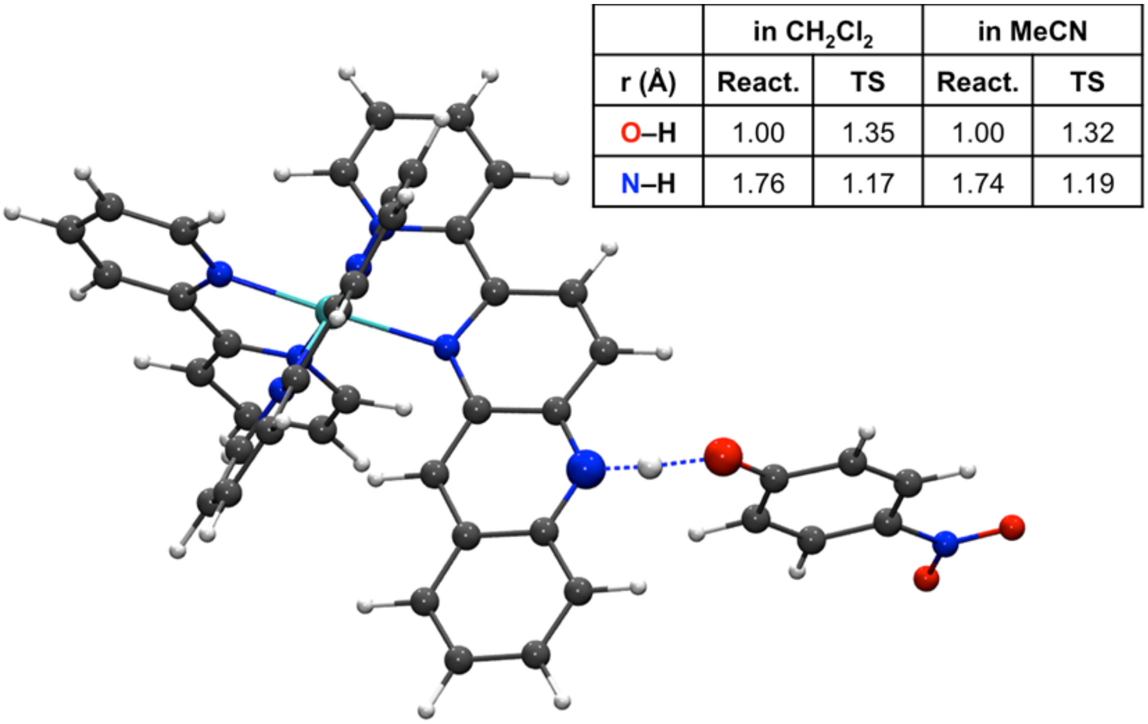

	in CH_2Cl_2		in MeCN	
r (Å)	React.	TS	React.	TS
O–H	1.00	1.35	1.00	1.32
N–H	1.76	1.17	1.74	1.19

Figure S3.3. Optimized structure of the adiabatic proton transfer transition state in the H-bonded **1**(T)-nitrophenol exciplex. Color code: Ru, cyan; N, blue; O, red; C, gray; and H, white. The optimized transition state structures correspond to the PT activation free energy of 3.8 kcal/mol in CH_2Cl_2 and 2.1 kcal/mol in MeCN. For the deuterated phenols, the PT activation energies are 4.7 kcal/mol in CH_2Cl_2 and 3.0 kcal/mol in MeCN, which correspond to the respective PT KIEs of 4.7 and 4.8.

Section S4. Energetics of Alternative Proton-Loss Electron Transfer Mechanisms.

Standard free energy changes (kcal/mol) for the quenching step in a sequential proton-loss electron transfer (SPLET),

$$\mathbf{X}(\mathrm{T}) + \text{R-PhO}^- = \mathbf{X}^- + \text{R-PhO}^\bullet \qquad \Delta_{\mathrm{SPLET}}G^0 = 23.06\times[E^0(\mathrm{PhO}^{\bullet/-}) - E^0(\mathbf{X}(\mathrm{T})/\mathbf{X}^-)]$$

and for a concerted proton-loss electron transfer (CPLET),

$$\mathbf{X}(\mathrm{T}) + \text{R-PhOH} + \mathrm{CH_3CN} = \mathbf{X}^- + \text{R-PhO}^\bullet + \mathrm{CH_3CNH^+}$$

$$\Delta_{\mathrm{CPLET}}G^0 = 23.06\times[E^0(\mathrm{PhO}^{\bullet/-}) - E^0(\mathbf{X}(\mathrm{T})/\mathbf{X}^-)] + 1.364\times\mathrm{p}K_\mathrm{a}(\mathrm{PhOH})$$

Table S4.1. Standard free energy changes (kcal/mol) for SPLET and CPLET with complexes **1**, **1i**, and **2** (Chart S4.1) in MeCN.

R-	pK_a (PhOH)[a]	E^0 ($\mathrm{PhO}^{\bullet/-}$)[a]	Complex **1** $E^0(\mathbf{1}(\mathrm{T})/\mathbf{1}^-) = 0.60$[b, c]		Complex **1i** $E^0(\mathbf{1i}(\mathrm{T})/\mathbf{1i}^-) = 0.57$[b,1]		Complex **2** $E^0(\mathbf{2}(\mathrm{T})/\mathbf{2}^-) = 0.71$[b]	
			$\Delta_{\mathrm{SPLET}}G^0$	$\Delta_{\mathrm{CPLET}}G^0$	$\Delta_{\mathrm{SPLET}}G^0$	$\Delta_{\mathrm{CPLET}}G^0$	$\Delta_{\mathrm{SPLET}}G^0$	$\Delta_{\mathrm{CPLET}}G^0$
MeO-	29.2[g]	–0.48	–25.0	14.9	–24.3	15.6	–27.5	12.3
Ph-	27.2[g]	–0.25	–19.6	17.5	–18.9	18.2	–22.2	14.9
Cl-	25.4[19]	0.04	–12.9	21.8	–12.2	22.5	–15.4	19.3
NC-	22.7[20]	0.32	–6.3	24.6	–5.7	25.3	–8.9	22.1
$\mathrm{O_2N}$-	20.9[20]	0.48	–2.8	25.7	–2.1	26.4	–5.4	23.1

[a]From Table S2.3; [b]in V vs Fc+/0; [c]From Table S3.4.

Chart S4.1. Complexes **1**, **1i** (a structural isomer of **1** with sterically screened uncoordinated N atom, which exhibits no photoinduced reactivity toward phenols),[1] and **2**.

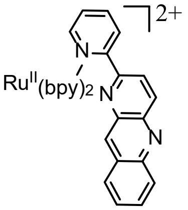

Complex **1**

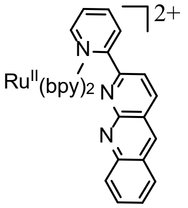

Complex **1i**

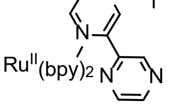

Complex **2**

Section S5. Kinetic isotope effect on the EPT rate from DFT calculations for complex **1** in CH_2Cl_2.

Nonadiabatic EPT rate constants. The nonadiabatic EPT rate constants for a fixed proton donor-acceptor distance (between phenol's O atom and ligand's N atom of complex **1**, R_{NO}) have been calculated using the following equation,[29]

$$k^{\mathrm{EPT}}(\Delta G_{00}; \lambda;\ R_{\mathrm{NO}}) = \sum_{\mu} P_{\mu} \sum_{\nu} \frac{\left|V_{\mathrm{el}} S_{\nu\mu}\right|^2}{\hbar} \sqrt{\frac{\pi}{\lambda k_{\mathrm{B}} T}}\ exp\left[-\frac{(\Delta G_{\nu\mu} + \lambda)^2}{4\lambda k_{\mathrm{B}} T}\right] \qquad \text{(S5.1)}$$

where the double summation is over all pairs of reactant/product electron-proton vibronic states μ/ν, P_{μ} is the Boltzmann probability of a reactant vibronic state μ, V_{el} is the electronic coupling (taken as unity for the H/D isotope effect calculations), $S_{\nu\mu}$ is the overlap integral between the proton vibrational wave functions for ν and μ, λ is the reorganization energy, k_B and $\hbar$ are the Boltzmann and Plank constants, respectively, T is the bath temperature set to 298.15 K, and $\Delta G_{\nu\mu}$ is the EPT reaction free energy involving the reactant/product vibrational levels μ/ν; with $\mu = \nu = 0$, the ΔG_{00} value closely corresponds (but not exactly identical) to the conventional reaction free energy. In equation S5.1, all P_{μ}, $S_{\nu\mu}$, and $\Delta G_{\nu\mu}$ are R_{NO}-dependent.

To account for the proton donor-acceptor thermal motion[30-33] and obtain the overall EPT rate constant, a series of $k^{EPT}(\Delta G_{00}, \lambda, R_{NO})$ calculated for a range of R_{NO} have been numerically integrated; that is,

$$k^{\mathrm{EPT}}(\Delta G_{00};\ \lambda) = \int_0^{\infty} P(R_{\mathrm{NO}})\, k^{\mathrm{EPT}}(\Delta G_{00}; \lambda;\ R_{\mathrm{NO}})\, dR_{\mathrm{NO}} \qquad \text{(S5.2)}$$

where $P(R_{NO})$ is the temperature-dependent probability of sampling a specific R_{NO} value, which serves as a weighting factor. Because $k^{EPT}(\Delta G_{00}, \lambda, R_{NO})$ is proportional to $S_{\nu\mu}^2$, KIE also changes with the square of the ratio of the vibrational wave functions overlaps for hydrogen and deuterium and is expected to increase as the overlaps decrease. However, the combined summation over all pairs of reactant/product vibronic states and the integration over R_{NO} leads to a more complex behavior.

Vibrational wave functions and diabatic proton potentials. The diabatic potential energy surfaces were computed to generate the proton vibrational wave functions, which in turn have been employed to compute $S_{\nu\mu}^2$ terms in equation S5.1. The individual steps involved in these computations were as flows:[34]

A. Structures corresponding to the saddle points on the adiabatic energy profiles along the N-H distance in the **1**(T)-phenol H-bonded exciplexes were obtained through a series of constrained geometry optimizations as described in the caption to Figure S3.2.

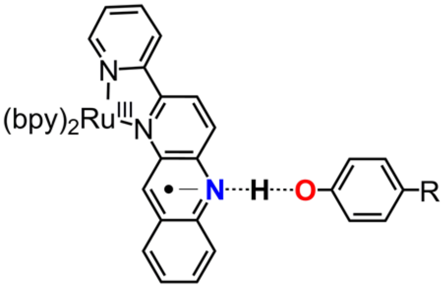

Saddle Point Structures

B. A series of structures were generated for several R_{NO} in 0.1 Å increments around the equilibrium R_{NO} distances of 2.76 and 2.81 Å in **1**(T)-nitrophenol and **1**(T)-methoxyphenol exciplex, respectively, using the approximate saddle point structures and translating **1**(T) and phenol molecules as rigid bodies along the donor acceptor axis. For each R_{NO}, an optimization of the proton position was performed, while holding the positions of all other atoms fixed. This was

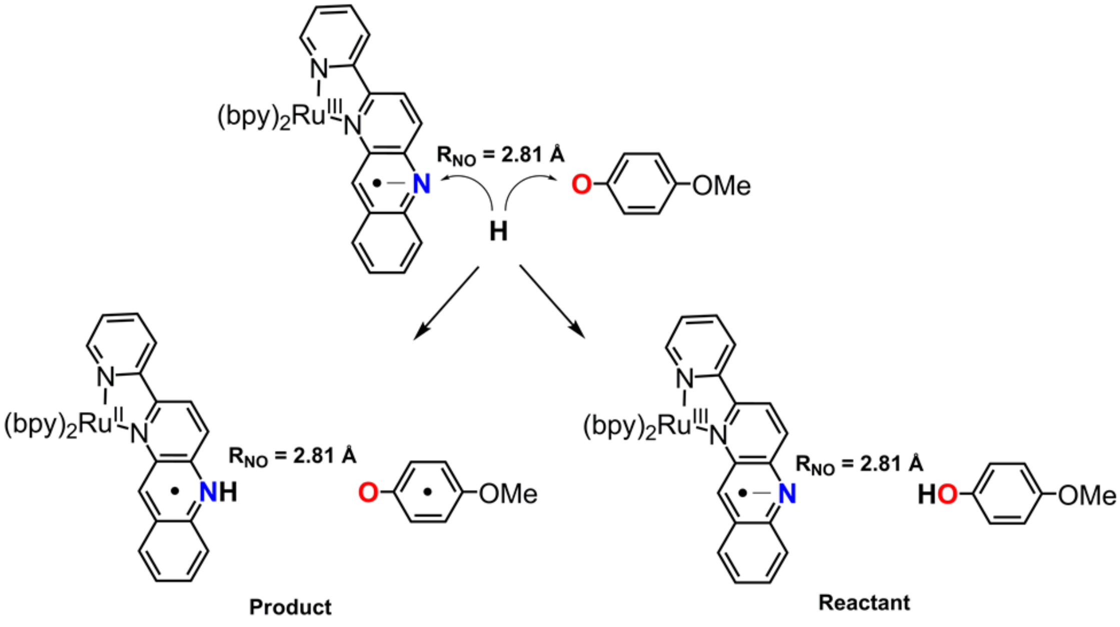

done by initially placing the proton close to the phenol's O atom or to the ligand's quinoline N atom of **1**(T) to obtain the reactant and product structures, respectively. This procedure is illustrated below,

C. For each pair of reactant and product structures obtained in step B for a specific R_{NO} distance, a line connecting the reactant's and product's protons defined a proton coordinate axis whose origin was placed in the middle. The diabatic potential energy surfaces for the reactant and product states (with respect to electron transfer; Scheme S5.1) were generated on a one-dimensional grid with ~0.05 Å spacing along this axis using Q-Chem software package version 4.2.1,[35]

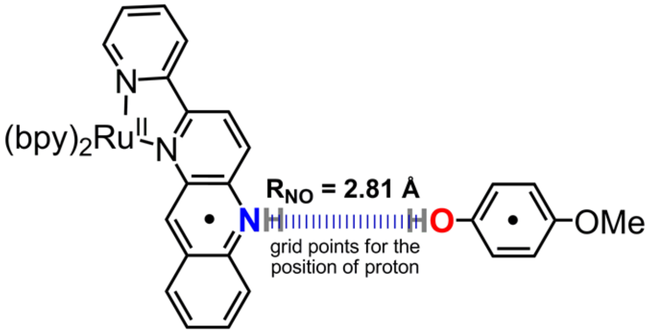

Specifically, constrained DFT (CDFT)[36] calculations at the M06 level of theory[37-39] with the IEFPCM continuum solvation model[40, 41] for CH_2Cl_2 using the Stuttgart [8s7p6d2f | 6s5p3d2f] ECP28MWB contracted pseudopotential basis set[42] on Ru and the 6-31G(d) basis set[43] on all other atoms were performed at each grid point for reactant and product states.

D. The resulting energies from step C were interpolated to generate smooth diabatic potential energy curves shown in Figures S5.2A-G and S5.3A-G, which have been used to determine the proton vibrational wave functions (also shown in Figures S5.2A-G and S5.3A-G) and compute the $S_{\mu\nu}^2$ values for the rate constant calculations via equation S5.1.

Scheme S5.1. Diabatic states associated with EPT from *p*-substituted phenols (R = MeO-, O_2N-) to **1**(T). The reactants and products in terms of the electron transfer are shown on the left in blue and red, respectively, and the fragments employed in CDFT calculations are depicted on the right.

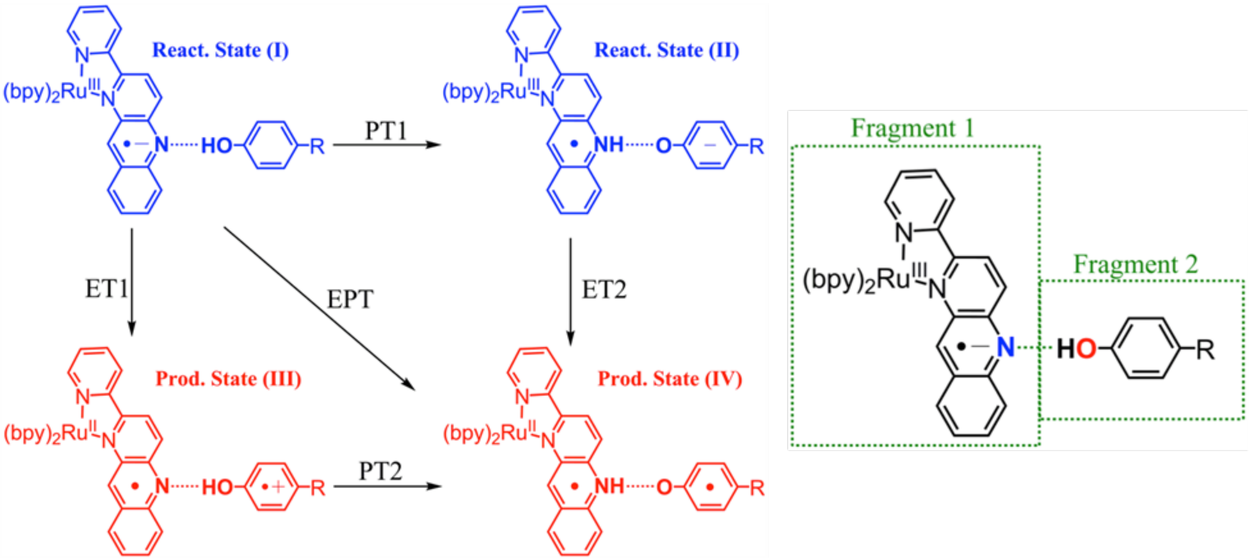

Fig. S5.1A, see caption on p. S35

$R_{\mathrm{NO}} = 2.51$ Å

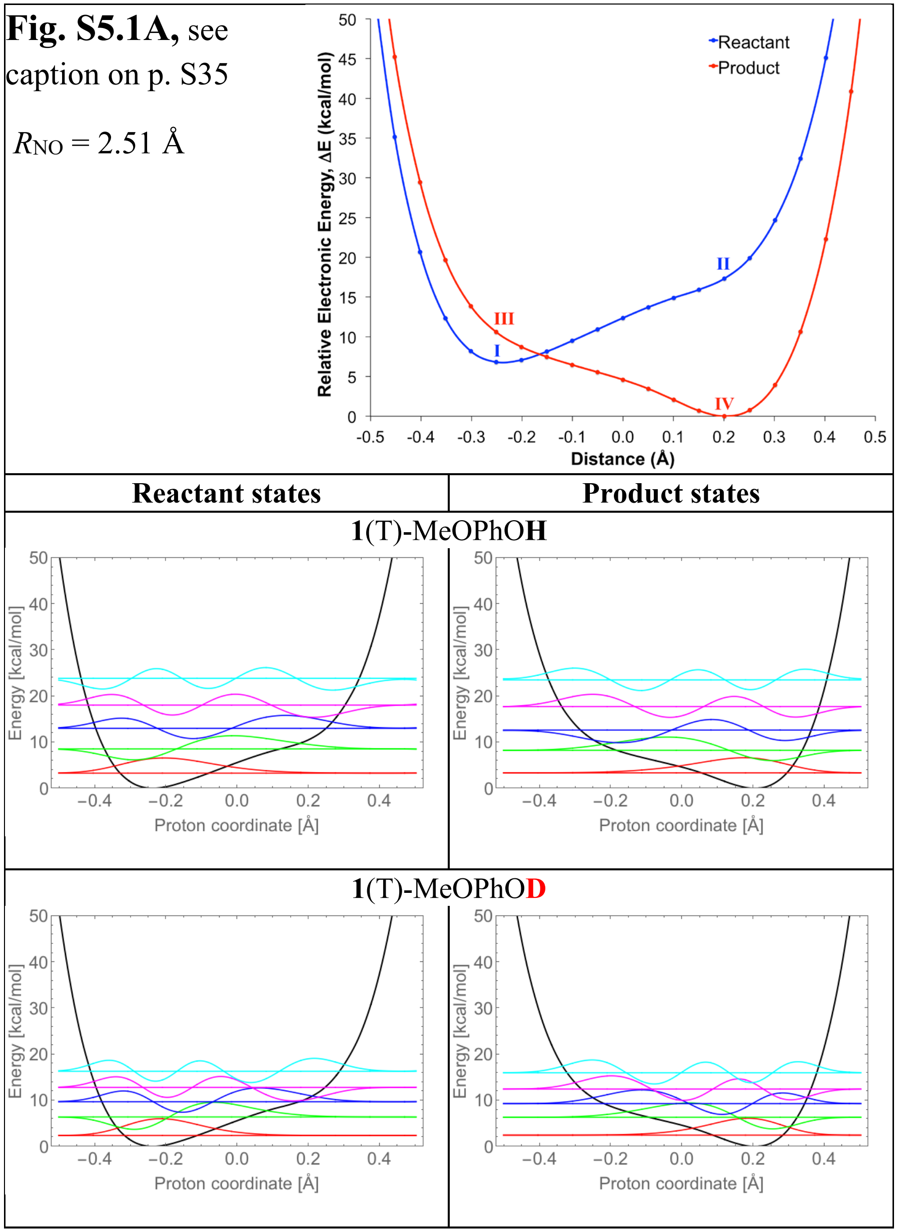

Fig. S5.1B, see caption on p. S35

$R_{\mathrm{NO}} = 2.61$ Å

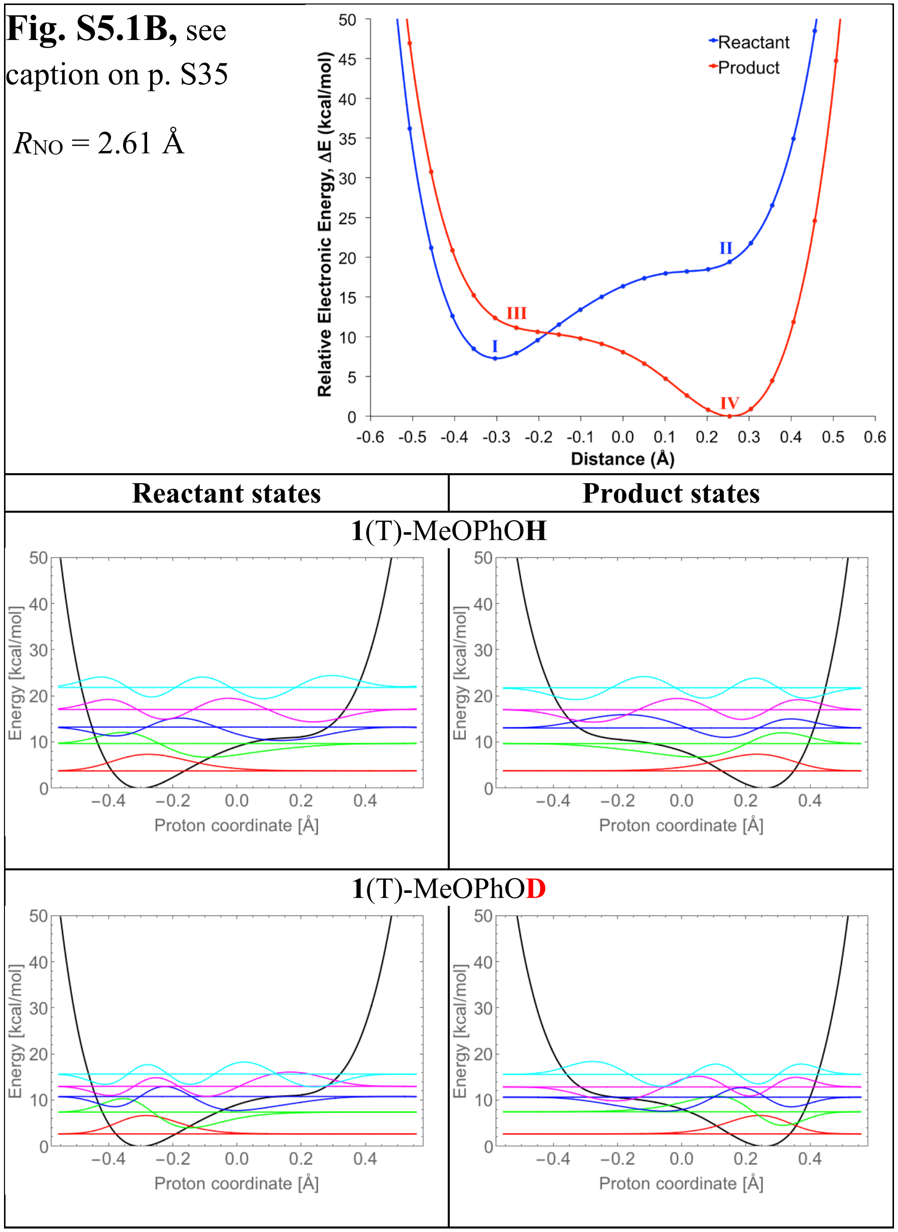

Fig. S5.1C, see caption on p. S35

$R_{\mathrm{NO}} = 2.71$ Å

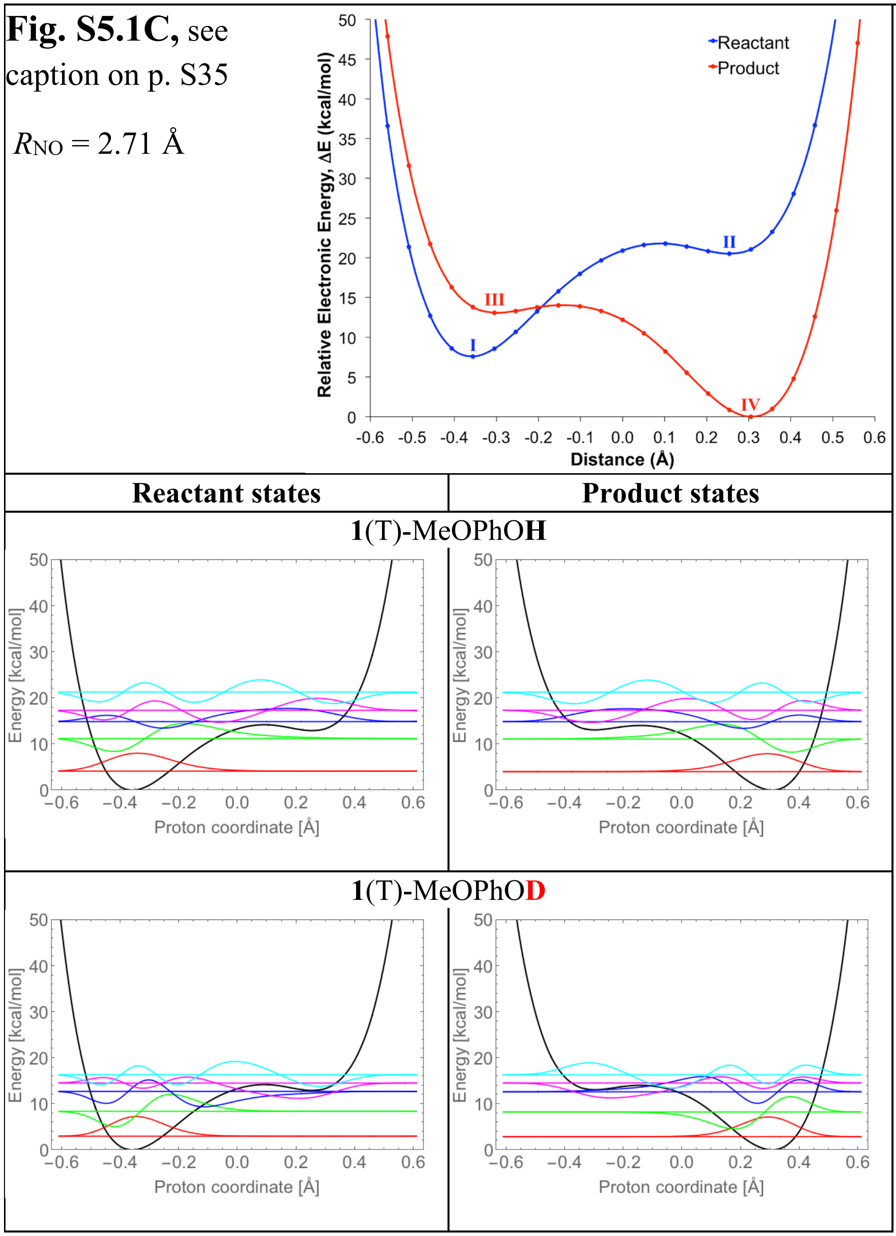

Fig. S5.1D, see caption on p. S35

$R_{\mathrm{NO}} = 2.81$ Å

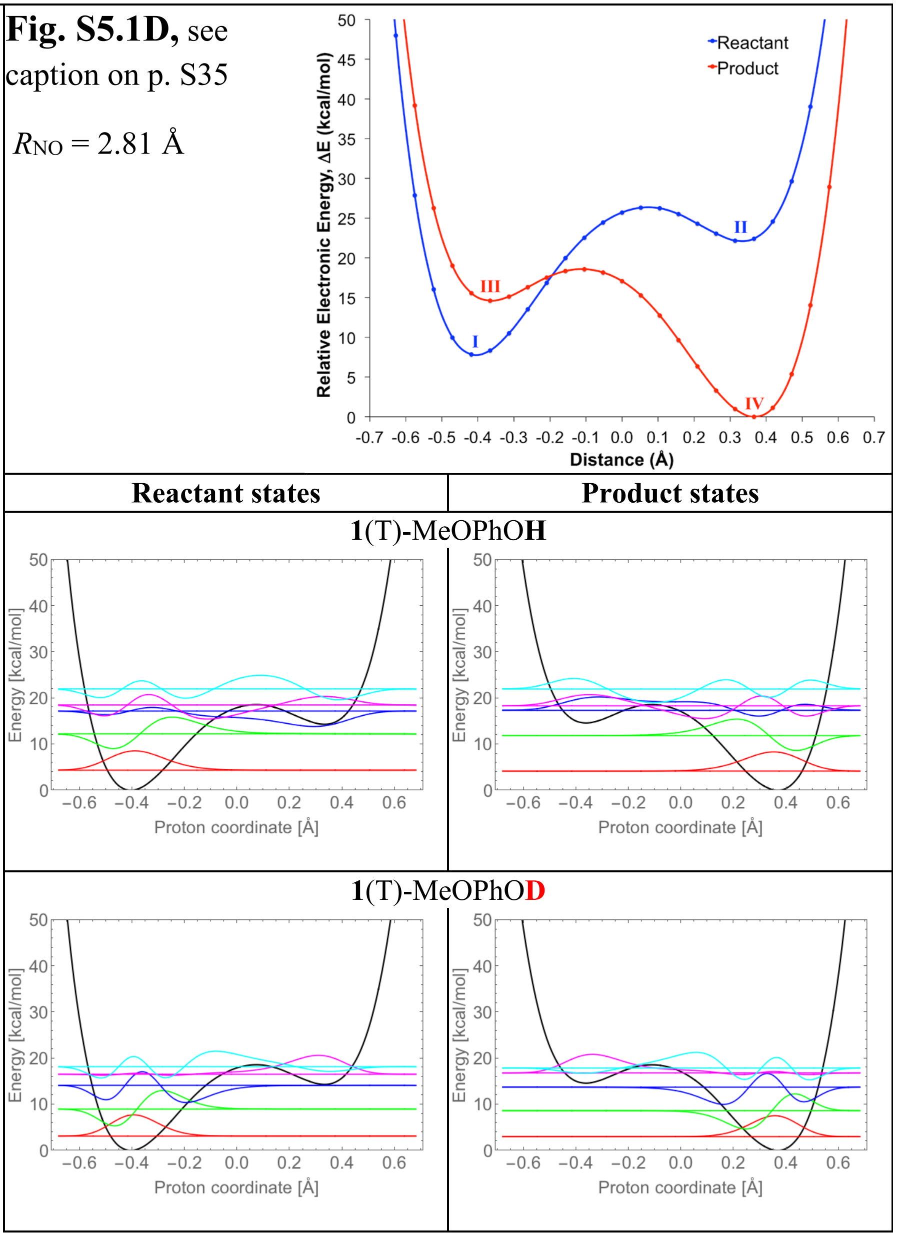

Fig. S5.1E, see caption on p. S35

R_{NO} = 2.91 Å

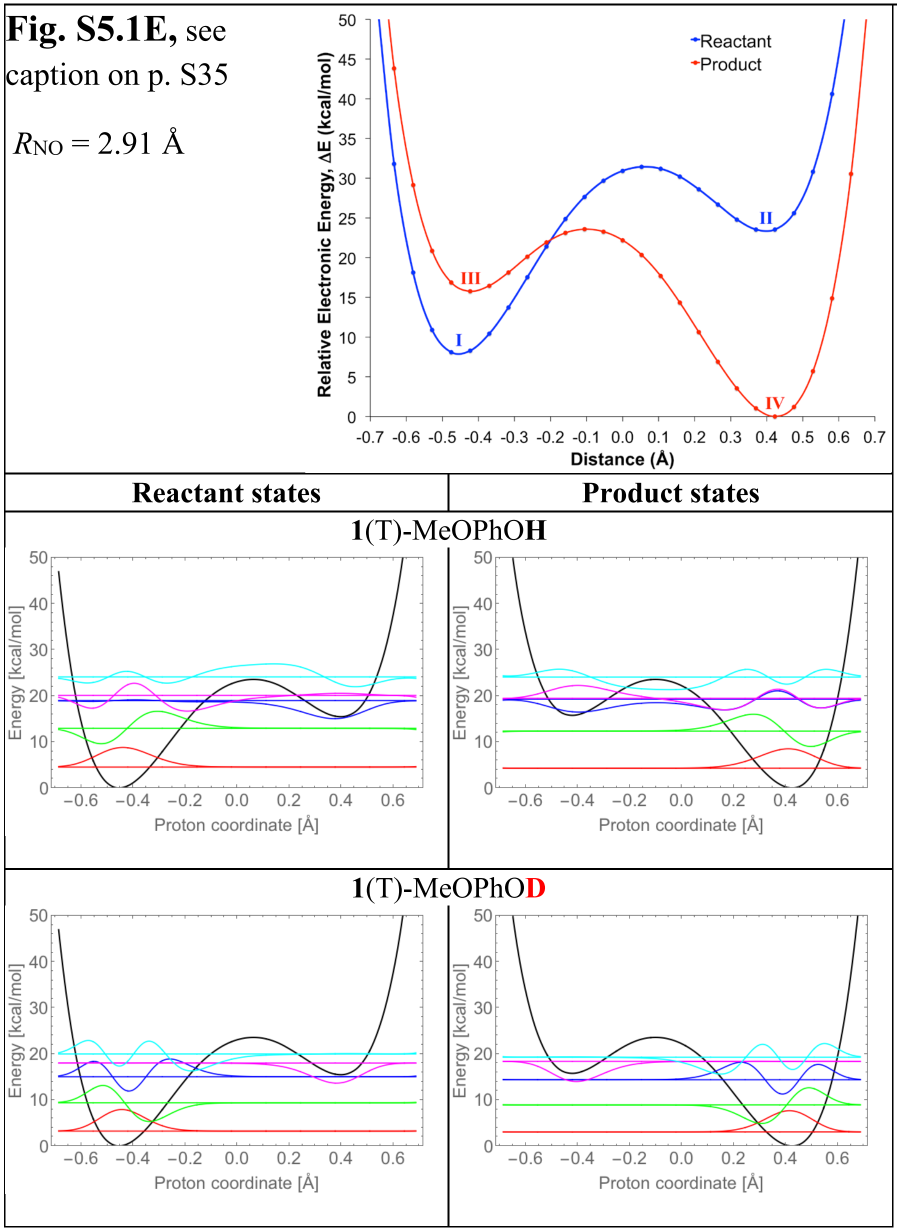

Reactant states

Product states

1(T)-MeOPhO**H**

1(T)-MeOPhO**D**

Fig. S5.1F, see caption on p. S35

R_{NO} = 3.01 Å

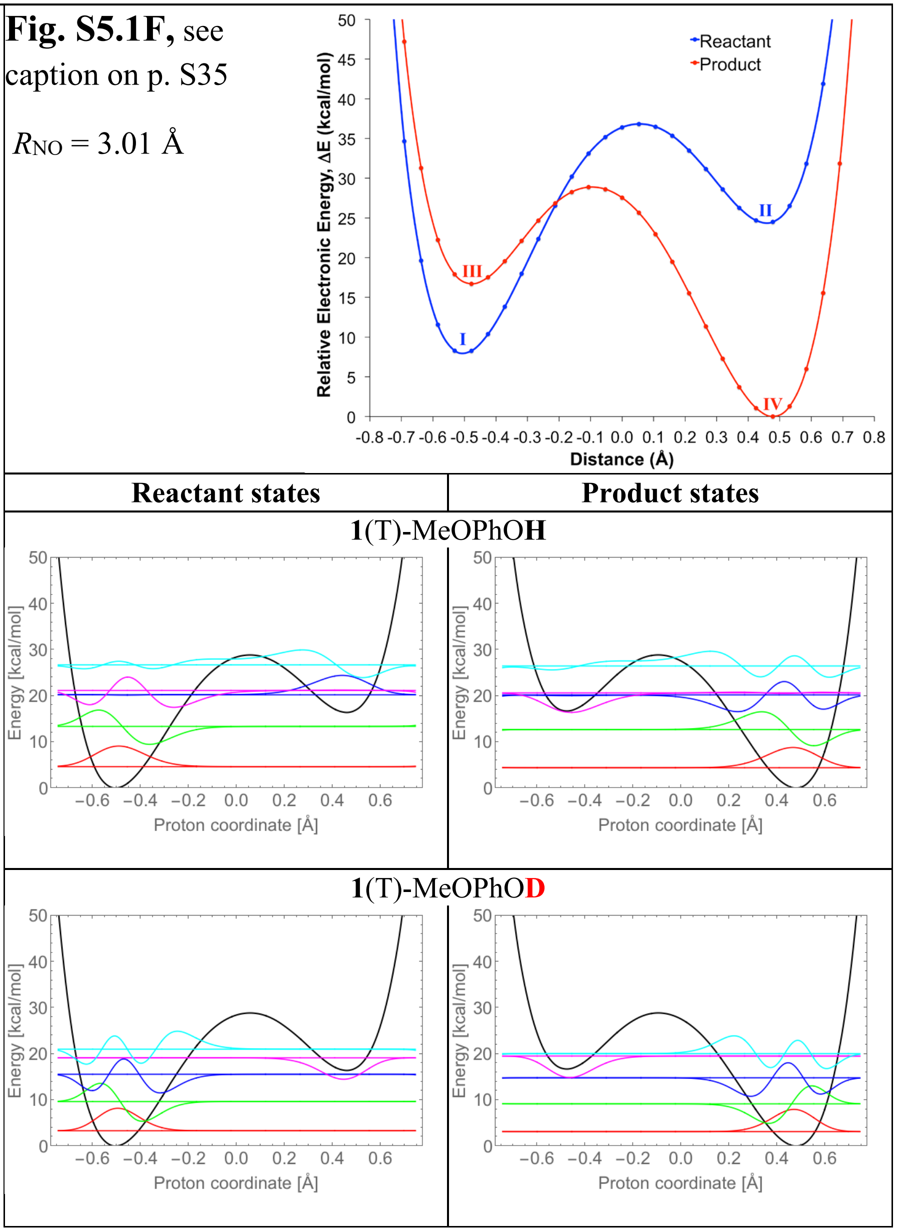

Reactant states

Product states

1(T)-MeOPhO**H**

1(T)-MeOPhO**D**

Fig. S5.1G

$R_{NO} = 3.11$ Å

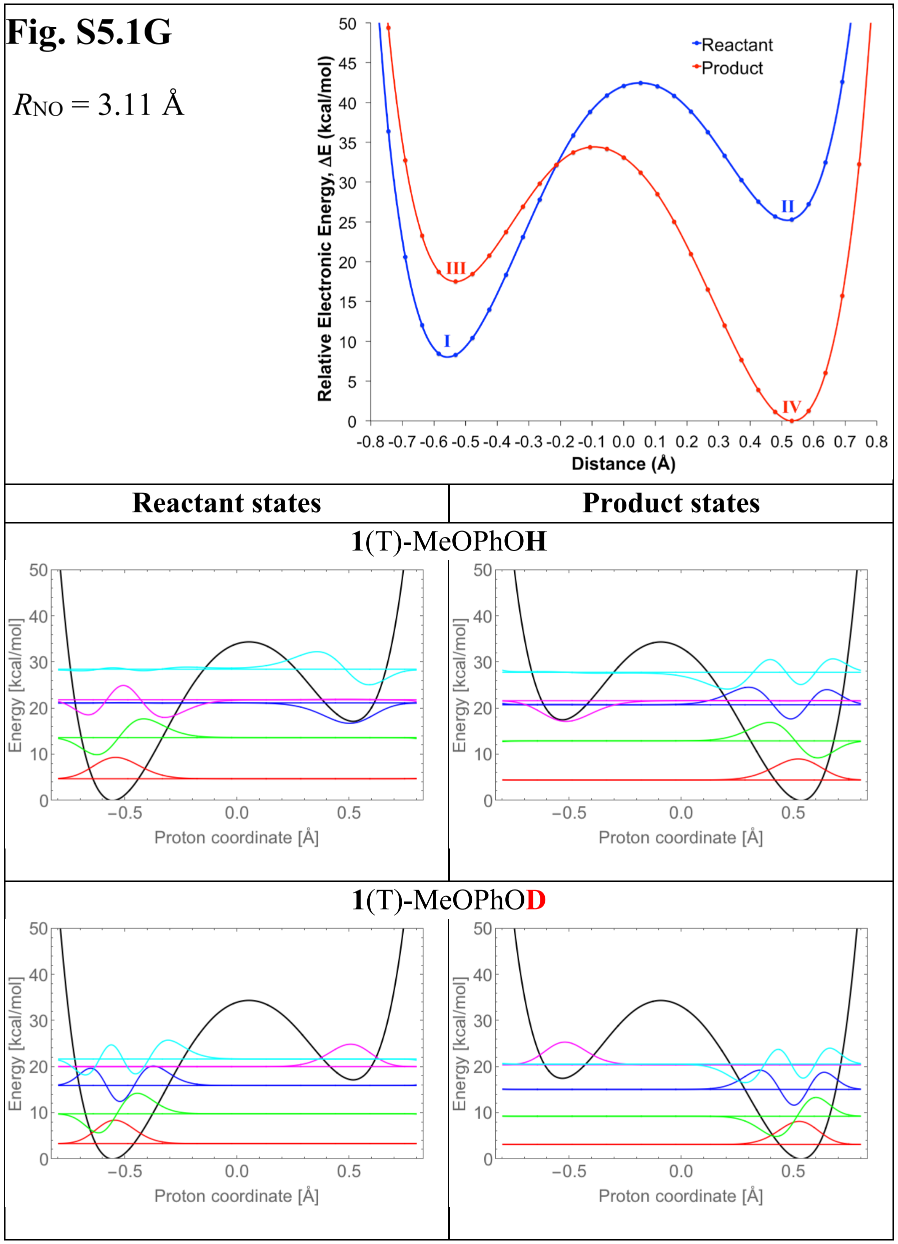

Figure S5.1A-G. Computed diabatic potential energy profiles for reactant and product states of **1**(T)-methoxyphenol in CH_2Cl_2 at the proton donor–acceptor distances of 2.51 (A), 2.61 (B), 2.71 (C), 2.81 (D, equilibrium distance), 2.91 (E), 3.01 (F), and 3.11 Å (G) and proton/deuteron vibrational wave functions for the reactant and product states (I)-(IV) in Scheme S5.1.

Fig. S5.2A, see caption on p. S39

$R_{NO} = 2.46$ Å

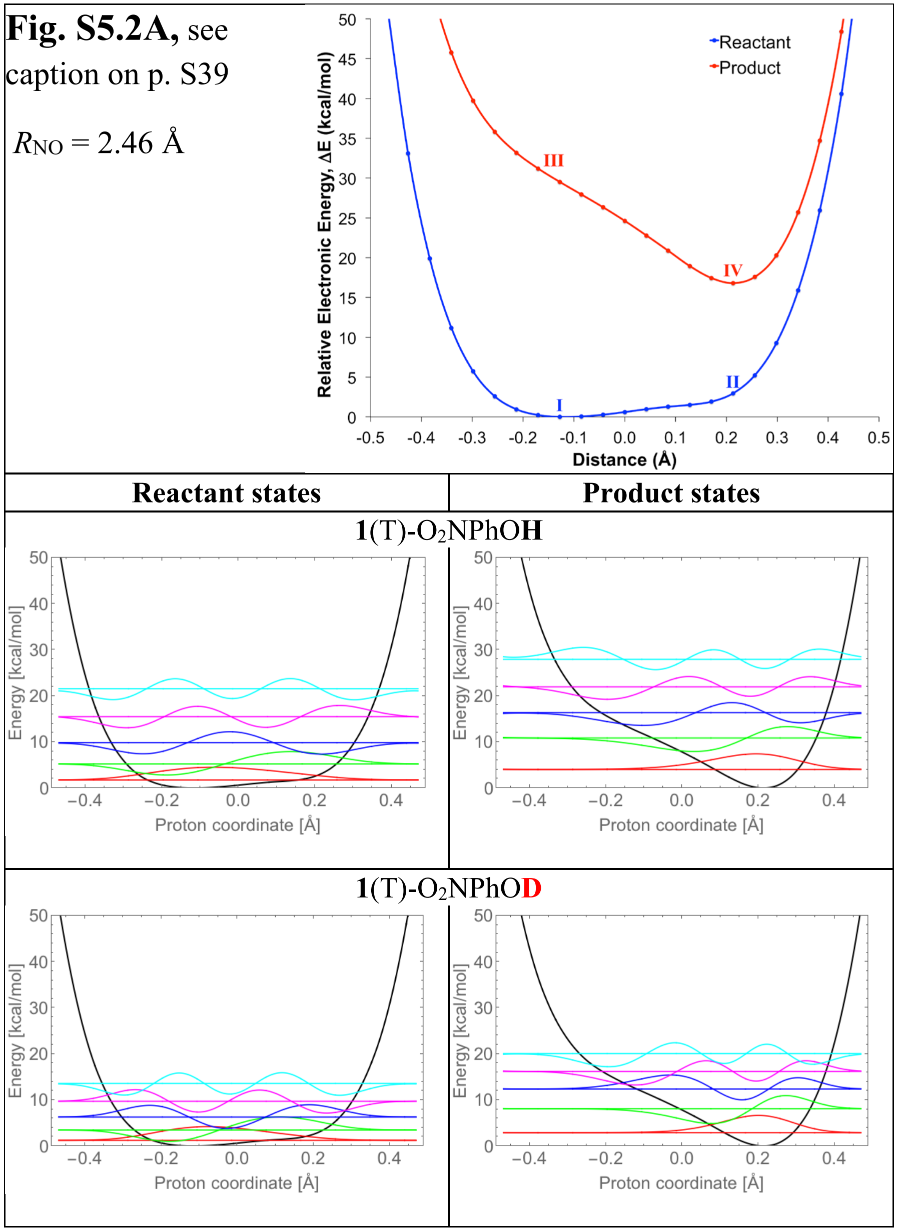

Fig. S5.2B, see caption on p. S39

$R_{NO} = 2.56$ Å

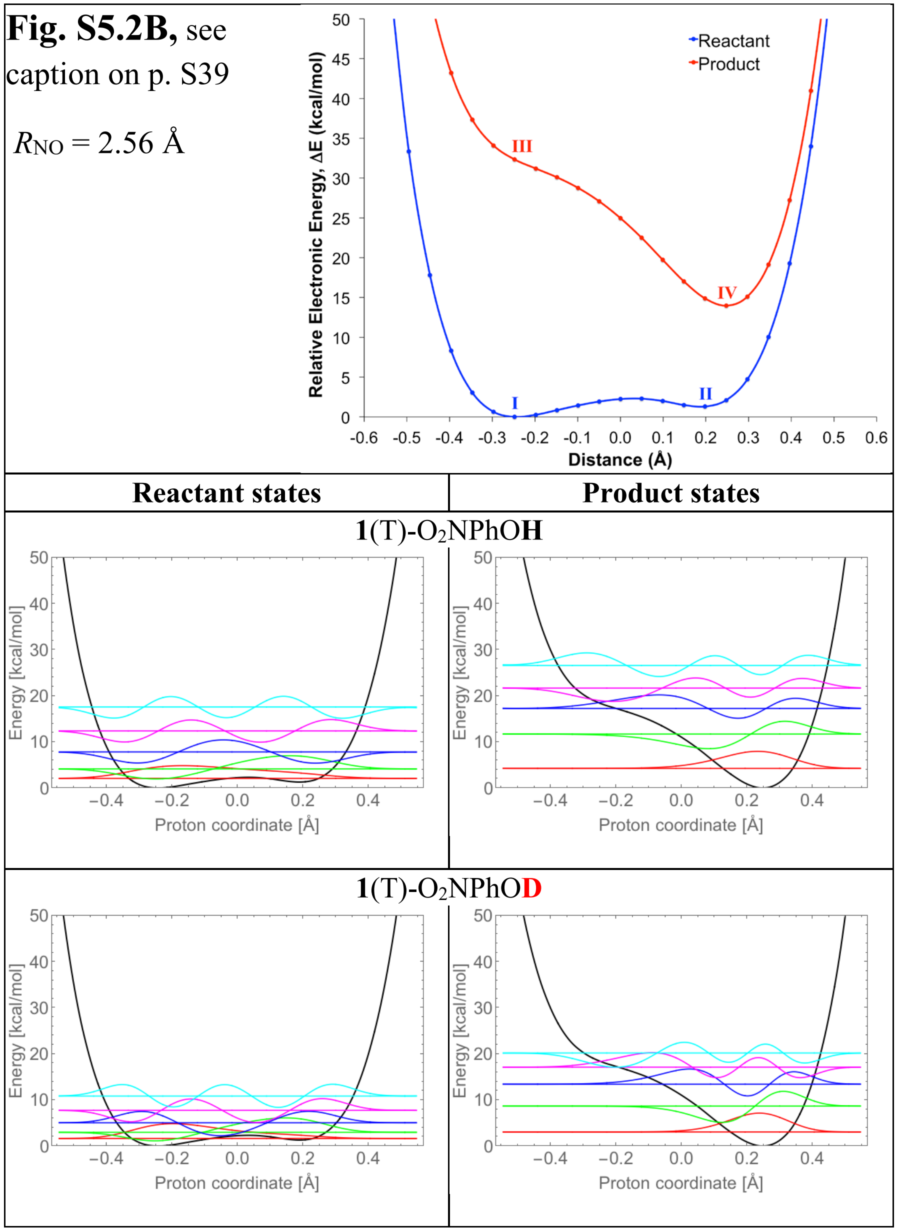

Fig. S5.2C, see caption on p. S39

$R_{\mathrm{NO}} = 2.66$ Å

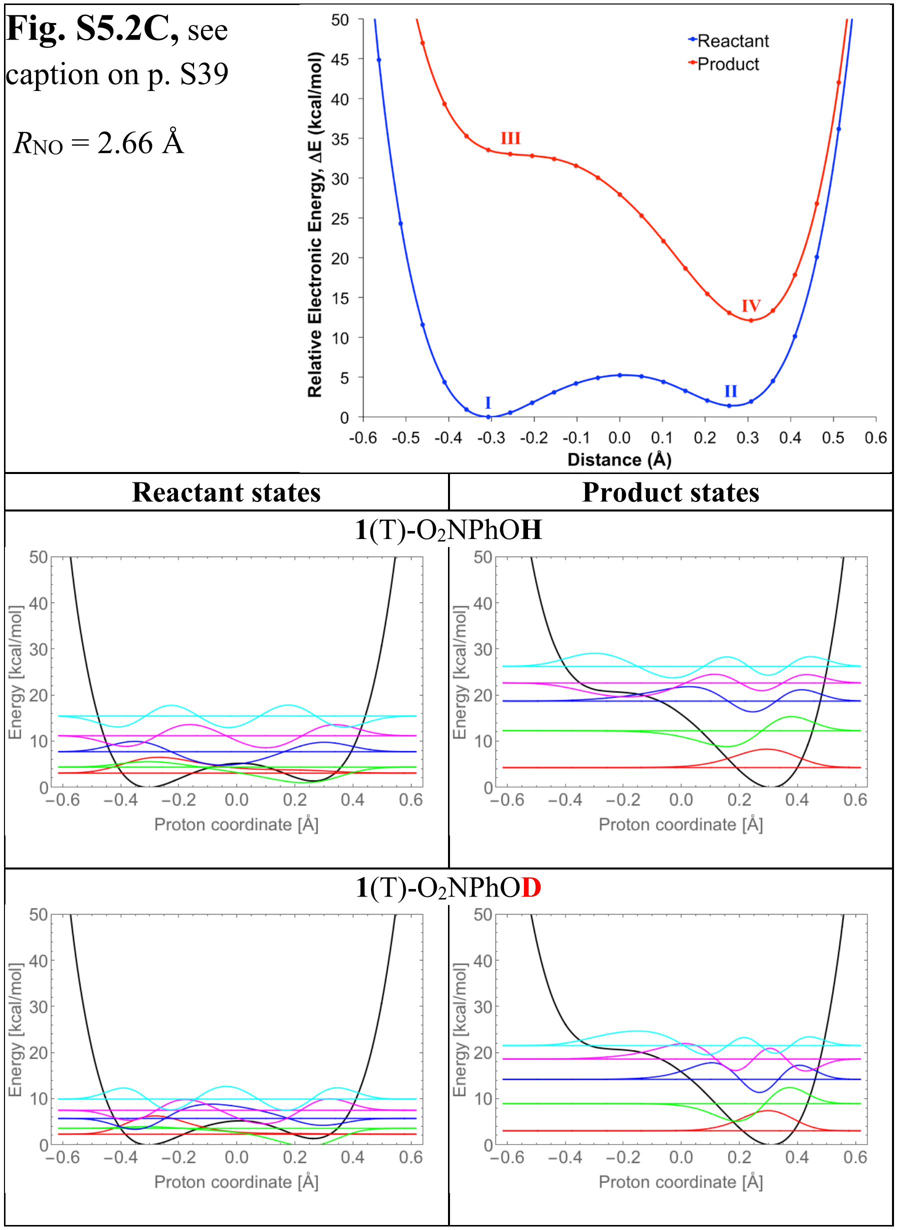

Fig. S5.2D, see caption on p. S39

$R_{\mathrm{NO}} = 2.76$ Å

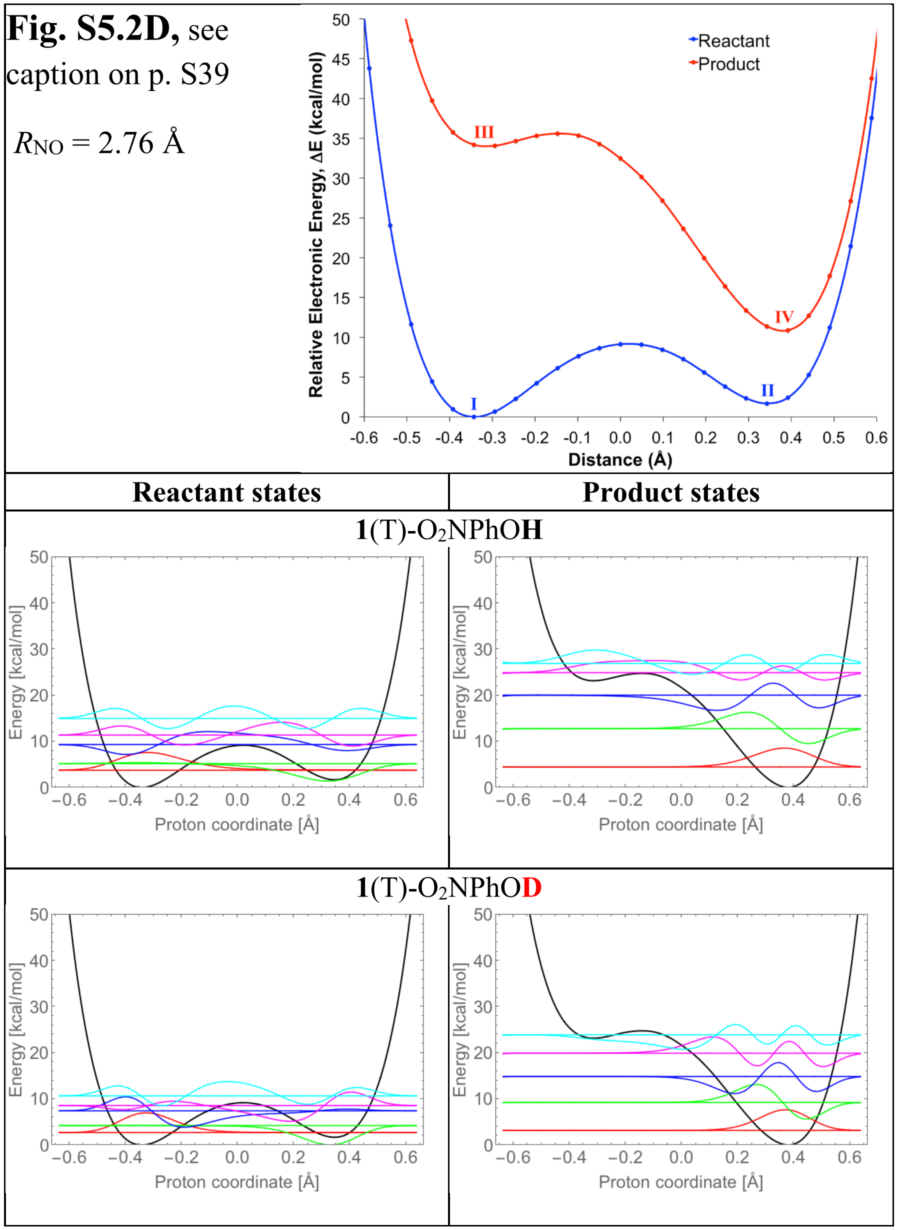

Fig. S5.2E, see caption on p. S39

$R_{NO} = 2.86$ Å

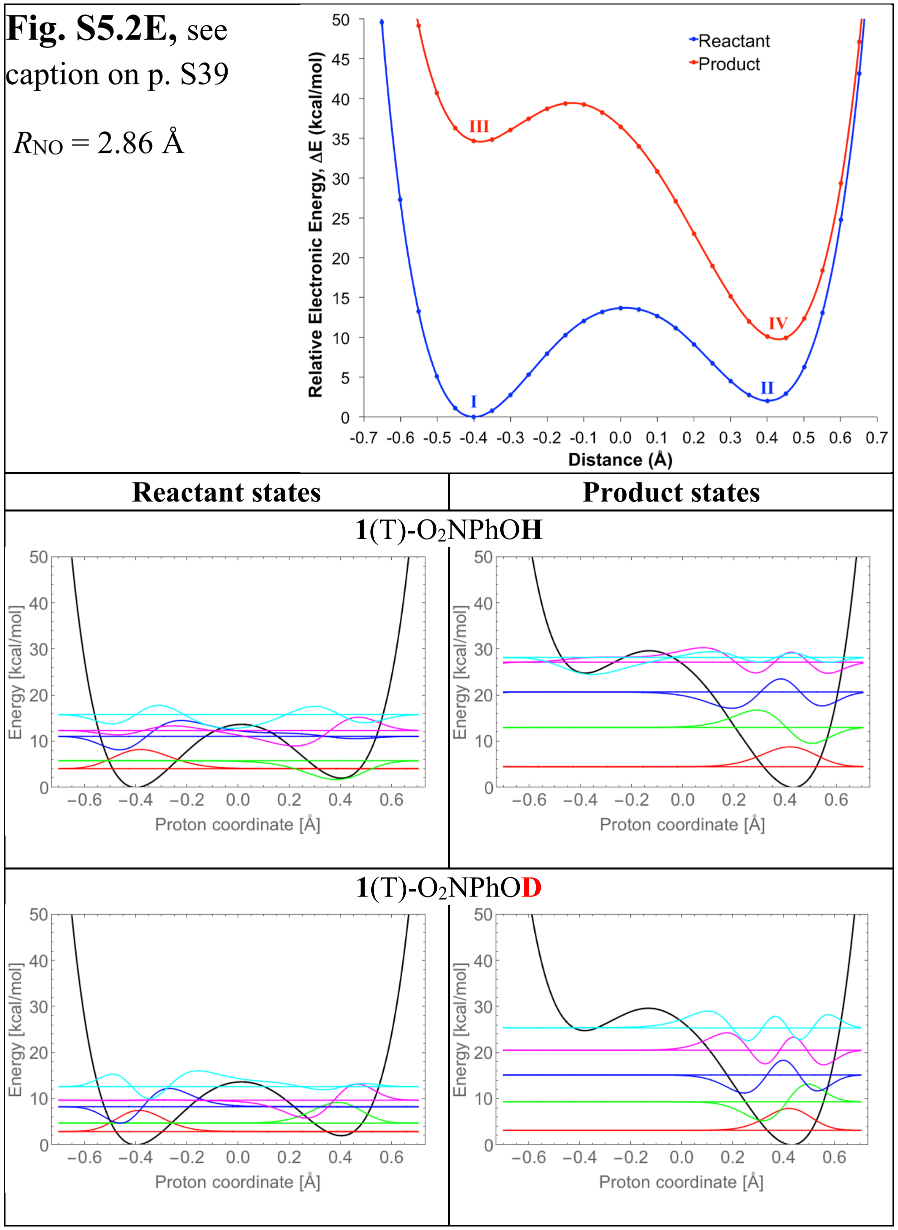

Fig. S5.2F, see caption on p. S39

$R_{NO} = 2.96$ Å

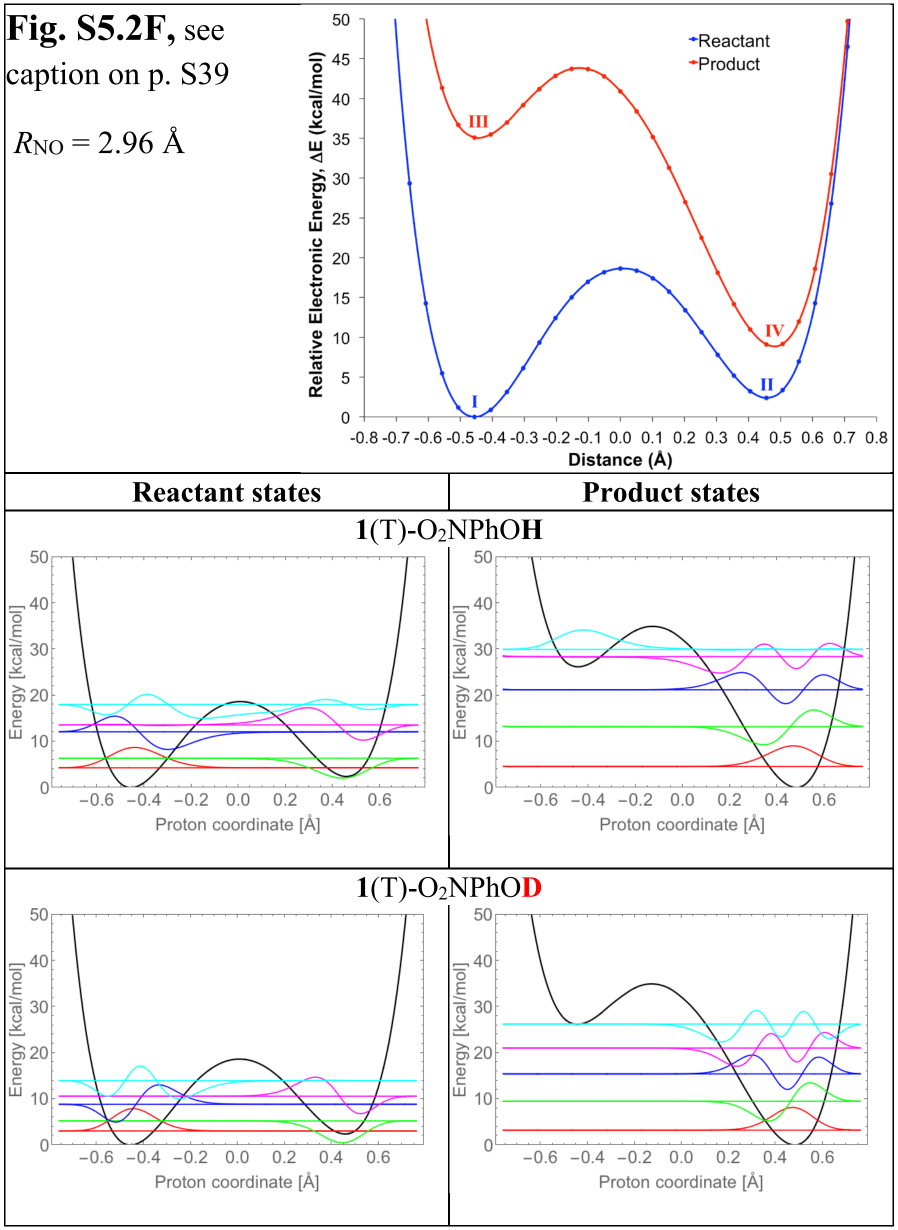

Fig. S5.2G

R_{NO} = 3.06 Å

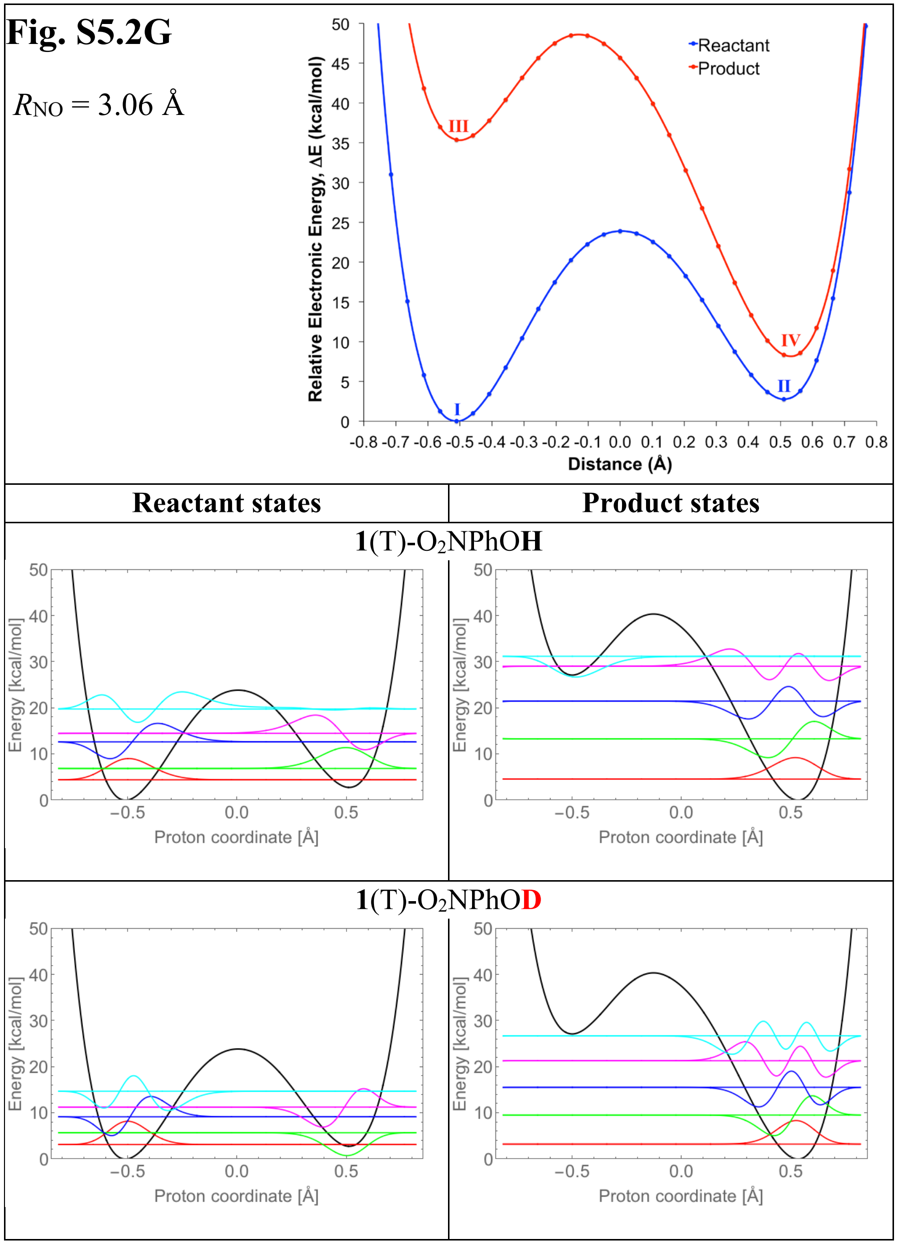

Figure S5.2A-G. Computed diabatic potential energy profiles for reactant and product states of **1**(T)-nitrophenol in CH_2Cl_2 at the proton donor–acceptor distances of 2.46 (A), 2.56 (B), 2.66 (C), 2.76 (D, equilibrium distance), 2.86 (E), 2.96 (F), and 3.06 Å (G) and proton/deuteron vibrational wave functions for the reactant and product states (I)-(IV) in Scheme S5.1.

Boltzmann probabilities, $P(R_{\mathrm{NO}})$. These temperature-dependent probabilities of finding the EPT donor and acceptor separated by R_{NO} appear in the equation S5.2 for $k^{\mathrm{EPT}}(\Delta G_{00}, \lambda)$ and are given by the classical harmonic probability distribution function,

$$P(R_{\mathrm{NO}}) = \sqrt{\frac{k_{\mathrm{eff}}}{2\pi k_{\mathrm{B}}T}}\, exp\left[-\frac{k_{\mathrm{eff}}(R_{\mathrm{NO}} - \bar{R}_{\mathrm{NO}})^2}{2k_{\mathrm{B}}T}\right] \qquad \text{(S5.3)}$$

where k_{eff} is an effective force constant for the mutual motion of the H-bonded reactants along the N-H-O axis. The k_{eff} values were evaluated via the parabolic fits to the computed energy profiles in Figure S5.4, which gave 0.079 hartree/Å^2 for **1**(T)-methoxyphenol and 0.083 hartree/Å^2 for **1**(T)-nitrophenol in CH_2Cl_2.

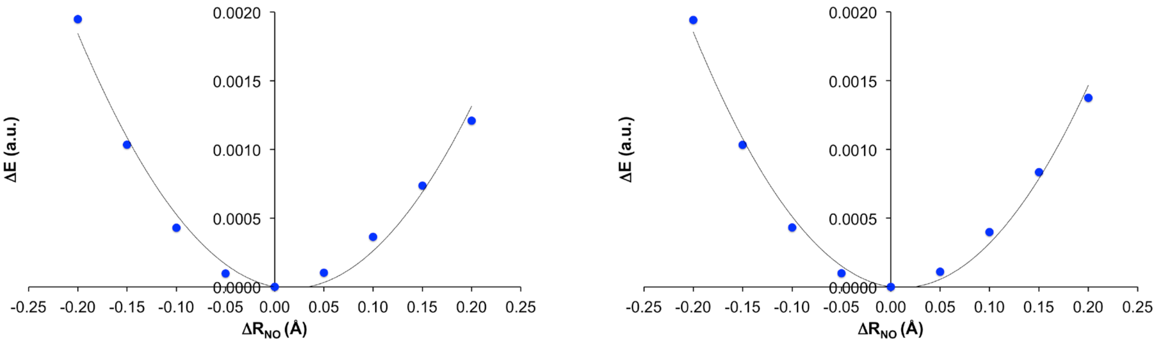

Figure S5.3. Energy profiles for the donor-acceptor mutual motion along the N-H-O axis in the **1**(T)-methoxyphenol (left) and **1**(T)-nitrophenol (right) H-bonded exciplexes. Both ΔE and ΔR_{NO} are relative to the corresponding quantities at equilibrium. The computed ΔE values (solid circles) were obtained through constrained optimizations of the H-bonded structures in CH_2Cl_2 via scanning along R_{NO}. The force constants k_{eff} = 0.0790 hartree/Å^2 for *p*-methoxyphenol and k_{eff} = 0.0830 hartree/Å^2 for *p*-nitrophenol were evaluated from the parabolic fits (smooth lines).

Reorganization energy and KIE. The total reorganization energy for the EPT reaction, λ, is the sum of the outer-sphere (solvent) reorganization energy λ_s and the inner-sphere (solute) reorganization energy λ_i. We have evaluated λ_s for EPT in CH_2Cl_2 using the following equation,

$$\lambda_s = \left(\frac{1}{2r_1} + \frac{1}{2r_2} - \frac{1}{R}\right) \times \left(\frac{1}{\epsilon_{\mathrm{op}}} - \frac{1}{\epsilon_{\mathrm{s}}}\right) \tag{S5.4}$$

where r_1 and r_2 are the radii of the equivalent spheres representing **1**(T) and phenol, R is the distance between the centers of these spheres, and ϵ_{s} and ϵ_{op} are the static and optical dielectric constants of the solvent taken to be 8.93 and 2.028, respectively. Using r_1 = 5.50 Å, r_2 = 2.76 Å, and R = 7.90 Å estimated from the optimized geometries of **1**(T)-methoxyphenol and **1**(T)-nitrophenol H-bonded exciplexes, we calculated λ_{s} = 1.53 eV (35.2 kcal/mol). For calculating λ_{i}, the standard expression,[44, 45]

$$\lambda_i = \frac{1}{2}\left[E_{ox}\left(R_{eq}^{red}\right) - E_{ox}\left(R_{eq}^{ox}\right) + E_{red}\left(R_{eq}^{ox}\right) - E_{red}\left(R_{eq}^{red}\right)\right] \tag{S5.5}$$

was used. Here, the individual terms are defined as follows:

$E_{ox}\left(R_{eq}^{red}\right)$	Electronic energy of PhO$^{\bullet}$ obtained on the optimized PhOH geometry via removing the phenolic hydrogen atom (proton and electron)
$E_{ox}\left(R_{eq}^{ox}\right)$	Electronic energy of PhO$^{\bullet}$ obtained on the optimized PhO$^{\bullet}$ geometry
$E_{red}\left(R_{eq}^{ox}\right)$	Electronic energy of **1**-H obtained on the optimized **1**(T) geometry via placing a hydrogen atom (proton and electron) on to the ligand's quinoline N atom of **1**(T); the optimization of the proton position was performed while holding the positions of all other atoms fixed
$E_{red}\left(R_{eq}^{red}\right)$	Electronic energy of **1**-H obtained on the optimized **1**-H geometry

These electronic energies were calculated at the M06 level of theory using the def2-TZVPP basis set on Ru and the def2-TZVP basis set on all other atoms. The computed λ_{i} were 0.34 eV (7.9 kcal/mol) and 0.30 eV (6.8 kcal/mol) for EPT reaction of **1**(T) with *p*-methoxy- and *p*-nitrophenol respectively, which gives the $\lambda = \lambda_{\mathrm{s}} + \lambda_{\mathrm{i}}$ values of 1.87 eV (43.0 kcal/mol) and 1.83 eV (42.0 kcal/mol) for EPT reaction of **1**(T) with *p*-methoxy and *p*-nitrophenol, respectively.

With the computed ΔG_{00} for the EPT reaction in CH_2Cl_2 (−13.5 kcal/mol for *p*-methoxyphenol and 1.9 kcal/mol for *p*-nitrophenol), these reorganization energies yield the deuterium KIE of 3.1 and 1.1 for EPT to **1**(T) from *p*-methoxy- and *p*-nitrophenol, respectively. The sensitivity of computed deuterium KIEs to the magnitudes of ΔG_{00} and λ can be evaluated from the data in Table S5.1, which shows a KIE invariance for *p*-nitrophenol in a wide range of these energies. For *p*-

methoxyphenol, the data in Table S5.1 suggest the KIE sensitivities of ~0.03 per kcal/mol in λ and ~0.2 per kcal/mol in ΔG_{00}.

Table S5.1. Dependence upon driving force (ΔG_{00}, kcal/mol) and reorganization energy (λ, kcal/mol) of computed H/D KIEs for EPT reaction from *p*-methoxy- and *p*-nitrophenol to **1**(T) in CH_2Cl_2.

ΔG_{00}	**λ = 35**	**λ = 40**	**λ = 45**	**λ = 50**	**λ = 55**
1(T)-methoxyphenol					
−10.5	3.6	3.8	3.9	4.0	4.1
−12.0	3.1	3.4	3.5	3.7	3.8
−13.5	2.8	3.0	3.2	3.4	3.5
−15.0	2.5	2.7	2.9	3.1	3.2
−16.5	2.2	2.4	2.6	2.8	3.0
1(T)-nitrophenol					
−1.1	1.1	1.1	1.1	1.1	1.1
0.4	1.1	1.1	1.1	1.1	1.1
1.9	1.1	1.1	1.1	1.1	1.1
3.4	1.1	1.1	1.1	1.1	1.1
4.9	1.1	1.1	1.1	1.1	1.1

Section S6. Products and Yields for Reactions of **1**(T) with *p*-MeO-PhOH and *p*-O_2N-PhOH in MeCN and CH_2Cl_2.

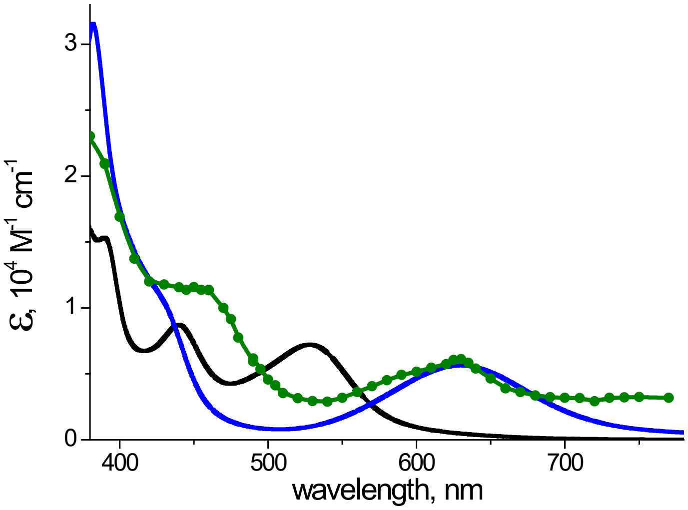

Figure S6.1. Absorption spectra of **1** in MeCN (black line), **1**-H^+ obtained by titrating **1** with $HClO_4$ in MeCN (blue line), and **1**-H obtained by sequential electron-proton addition to **1** using pulse radiolysis in water[46] (green symbols and line).

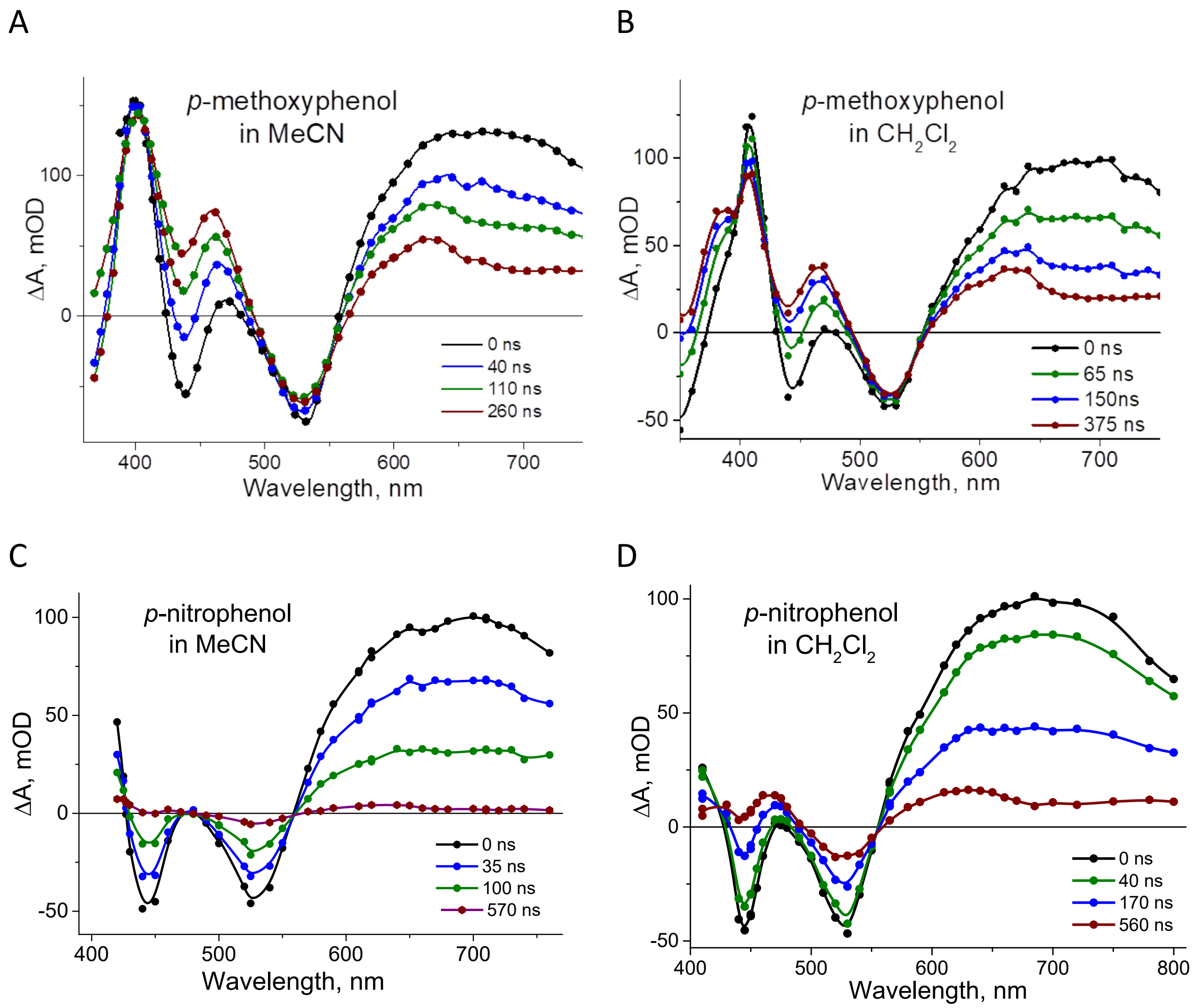

Figure S6.2. Transient absorption spectra recorded at the indicated times after 2 ns, 532 nm laser flash photolysis of complex **1** in: (A) MeCN containing 200 mM of *p*-methoxyphenol; (B) CH_2Cl_2 containing 7 mM of *p*-methoxyphenol; (C) MeCN containing 800 mM of *p*-nitrophenol; (D) CH_2Cl_2 containing 150 mM of *p*-nitrophenol. The prompt spectra at 0 ns are due to the difference between the spectrum of **1**(T**)** and that of **1** only. The final spectra correspond to the difference between absorptions by the separated products from the quenching reactions and that of **1** after the quenching completion, but before any subsequent second-order reactions between the products could occur. All solutions are Ar-purged.

Relative product yields.

In terms of Scheme 1 and eq 1-4 (main text), the aggregate yield (η_{prod}) of the nascent {**1**-H/PhO$^{\bullet}$} and {**1**(T)-H^{+}/PhO^{-}} pairs resulting from the concurrent EPT and ET quenching of **1**(T) by a phenol (caged RP and IP products in Scheme 1, main text) is given by,

$$\eta_{\text{prod}} = \frac{[\text{caged products}]}{[\mathbf{1}(\text{T})]_0} = \frac{k_{\text{q}} K_{\mathbf{1}\text{-P}}^{\text{app}}\,[\text{P}]_0}{(1+K_{\mathbf{1}\text{-P}}^{\text{app}}\,[\text{P}]_0)k_{\text{obs}}}$$

where $[\mathbf{1}(\text{T})]_0$ is the initial **1**(T) concentration created by flash photolysis and [caged products] refers to {**1**-H/PhO$^{\bullet}$} + {**1**(T)-H^{+}/PhO^{-}} generated over the course of **1**(T) decay. Considering that under the experimental conditions of flash photolysis $K_{\mathbf{1}\text{-P}}^{\text{app}}\,[\text{P}]_0 \ll 1$, we write,

$$\eta_{\text{prod}} = \frac{k_{\text{q}} K_{\mathbf{1}\text{-P}}^{\text{app}}\,[\text{P}]_0}{k_{\text{obs}}} = \frac{k_{\text{q}}^{\text{obs}}\,[\text{P}]_0}{k_0 + k_{\text{q}}^{\text{obs}}[\text{P}]_0} - \frac{k_0\left(k_0^{1\text{-P}}/k_0 - 1\right)K_{\mathbf{1}\text{-P}}^{\text{app}}\,[\text{P}]_0}{k_0 + k_{\text{q}}^{\text{obs}}[\text{P}]_0}$$

Because $k_{\text{q}}^{\text{obs}}\,[\text{P}]_0 > k_0$, and, as we have previously demonstrated,[1] $\left(k_0^{1\text{-P}}/k_0 - 1\right) < 1$, we can safely omit the second term on the right-hand side of the above equation and evaluate η_{prod} only through experimentally-available lifetime in the absence of a quencher (τ_0, Table S3.4) and bimolecular quenching rate constant ($k_{\text{q}}^{\text{obs}}$, Table 1, main text); that is,

$$\eta_{\text{prod}} = \frac{\tau_0 k_{\text{q}}^{\text{obs}}\,[\text{P}]_0}{1+\tau_0 k_{\text{q}}^{\text{obs}}[\text{P}]_0}$$

The so-obtained values of η_{prod} for experiments presented in Figure S6.2 are: 0.55 for panel A, 0.76 for panel B, 0.57 for panel C, and 0.55 for panel D.

These values together with the 680 nm amplitudes of spectra in Figure S6.2 recorded at 0 ns that are due to promptly generated **1**(T) have been used for normalizing the final spectra in that figure to the same $[\mathbf{1}(\text{T})]_0$ and η_{prod}. The results of this procedure shown in Figure 5, main text reflect the relative compositions and yields of separated products originating from the same $[\mathbf{1}(\text{T})]_0$ with the same chemical quenching efficiency

Section S7. Kinetic Solvent Effect for Complex **2**.

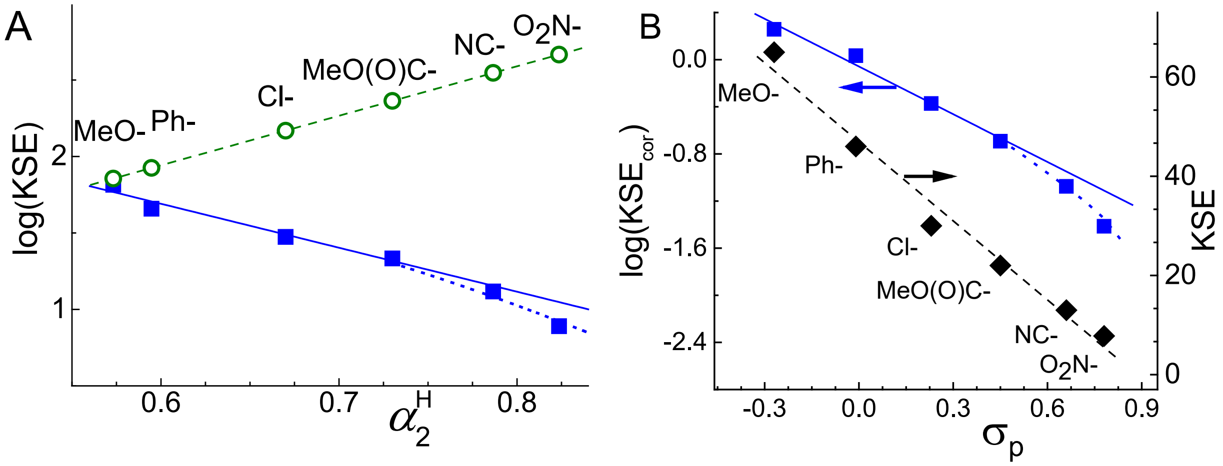

Figure S7.1. (A) Dependencies of logKSE on phenol's HB acidity for complex **1**: KSE predicted by eq 11, main text (circles and dashed line) and observed KSE from Table 1 (squares). (B) Dependencies of logKSE$_{cor}$ (eq 12, main text; squares) and observed KSE (diamonds and dashed line showing a linear fit) on σ_p. The solid lines give the linear fits through the leftmost 4 data points. The dotted lines serve as the visual aids only.

Section S8. References.

1. S. V. Lymar, M. Z. Ertem, A. Lewandowska-Andralojc and D. E. Polyansky, *J. Phys. Chem. Lett.*, 2017, **8**, 4043-4048.
2. D. D. Wagman, W. H. Evans, V. B. Parker, R. H. Schumm, I. Halow, S. M. Bailey, K. L. Churney and R. L. Nuttall, *J. Phys. Chem. Ref. Data*, 1982, **11, Suppl. 2**.
3. M. H. Abraham, P. L. Grellier, D. V. Prior, P. P. Duce, J. J. Morris and P. J. Taylor, *J. Chem. Soc., Perkin Trans. 2*, 1989, 699-711.
4. M. H. Abraham, P. L. Grellier, D. V. Prior, J. J. Morris and P. J. Taylor, *J. Chem. Soc., Perkin Trans. 2*, 1990, 521-529.
5. M. H. Abraham, *Chem. Soc. Rev.*, 1993, **22**, 73-83.
6. D. W. Snelgrove, J. Lusztyk, J. T. Banks, P. Mulder and K. U. Ingold, *J. Am. Chem. Soc.*, 2001, **123**, 469-477.
7. P. Mulder, H.-G. Korth, D. A. Pratt, G. A. DiLabio, L. Valgimigli, G. F. Pedulli and K. U. Ingold, *J. Phys. Chem. A*, 2005, **109**, 2647-2655.
8. J. J. Warren, T. A. Tronic and J. M. Mayer, *Chem. Rev.*, 2010, **110**, 6961-7001.
9. H. A. Schwarz, *J. Chem. Educ.*, 1981, **58**, 101.
10. E. Roduner, *Radiat. Phys. Chem.*, 2005, **72**, 201-206.
11. D. A. Armstrong, R. E. Huie, S. Lymar, W. H. Koppenol, G. Merényi, P. Neta, B. Ruscic, D. M. Stanbury, S. Steenken and P. Wardman, *Pure Appl. Chem.*, 2015, **87**, *1139-1150*.
12. E. Brunner, *J. Chem. Eng. Data*, 1985, **30**, 269-273.
13. Purwanto, R. M. Deshpande, R. V. Chaudhari and H. Delmas, *J. Chem. Eng. Data*, 1996, **41**, 1414-1417.
14. J. A. S. Roberts and R. M. Bullock, *Inorg. Chem.*, 2013, **52**, 3823-3835.
15. C. L. Young, ed., *Hydrogen and Deuterium*, Pergamon Press, Oxford, England, 1981.
16. I. M. Kolthoff and F. G. Thomas, *J. Phys. Chem.*, 1965, **69**, 3049-3058.
17. A. Albert and E. P. Serjeant, *The Determination of Ionization Constants*, Chapman and Hall, London, Third edn., 1984.
18. J. Lind, X. Shen, T. E. Eriksen and G. Merenyi, *J. Am. Chem. Soc.*, 1990, **112**, 479-482.
19. K. Izutsu, *Acid-base Dissociation Constants in Dipolar Aprotic Solvents*, Blackwell Scientific Publications, Oxford, First edn., 1990.
20. M. K. Chantooni and I. M. Kolthoff, *J. Phys. Chem.*, 1976, **80**, 1306-1310.
21. Y.-R. Luo, *Comprehensive Handbook of Chemical Bond Energies*, CRC Press, Boca Raton, 2007.
22. F. G. Bordwell and J. Cheng, *J. Am. Chem. Soc.*, 1991, **113**, 1736-1743.
23. B. W. Cohen, D. E. Polyansky, P. Achord, D. Cabelli, J. T. Muckerman, K. Tanaka, R. P. Thummel, R. F. Zong and E. Fujita, *Faraday Discuss.*, 2012, **155**, 129-144.
24. D. P. Rillema, G. Allen, T. J. Meyer and D. Conrad, *Inorg. Chem.*, 1983, **22**, 1617-1622.
25. V. V. Pavlishchuk and A. W. Addison, *Inorg. Chim. Acta*, 2000, **298**, 97-102.
26. N. J. Turro, *Modern Molecular Photochemistry*, University Science Books, Sausalito, 1991.
27. R. M. Fuoss, *J. Am. Chem. Soc.*, 1958, **80**, 5059-5061.
28. S. L. Murov, I. Carmichael and G. L. Hug, *Handbook of Photochemistry*, Marcel Dekker, New York, 2d edn., 1993.
29. A. Soudackov and S. Hammes-Schiffer, *J. Chem. Phys.*, 2000, **113**, 2385-2396.
30. S. Hammes-Schiffer, E. Hatcher, H. Ishikita, J. H. Skone and A. V. Soudackov, *Coord. Chem. Rev.*, 2008, **252**, 384-394.
31. S. J. Edwards, A. V. Soudackov and S. Hammes-Schiffer, *J. Phys. Chem. A*, 2009, **113**, 2117-2126.
32. B. Auer, L. E. Fernandez and S. Hammes-Schiffer, *J. Am. Chem. Soc.*, 2011, **133**, 8282-8292.
33. S. Horvath, L. E. Fernandez, A. V. Soudackov and S. Hammes-Schiffer, *Proc. Natl. Acad. Sci. U. S. A.*, 2012, **109**, 15663.

34. M. T. Huynh, S. J. Mora, M. Villalba, M. E. Tejeda-Ferrari, P. A. Liddell, B. R. Cherry, A.-L. Teillout, C. W. Machan, C. P. Kubiak, D. Gust, T. A. Moore, S. Hammes-Schiffer and A. L. Moore, *ACS Cent. Sci.*, 2017, **3**, 372-380.
35. Y. Shao, Z. Gan, E. Epifanovsky, A. T. B. Gilbert, M. Wormit, J. Kussmann, A. W. Lange, A. Behn, J. Deng, X. Feng, D. Ghosh, M. Goldey, P. R. Horn, L. D. Jacobson, I. Kaliman, R. Z. Khaliullin, T. Kuś, A. Landau, J. Liu, E. I. Proynov, Y. M. Rhee, R. M. Richard, M. A. Rohrdanz, R. P. Steele, E. J. Sundstrom, H. L. Woodcock, P. M. Zimmerman, D. Zuev, B. Albrecht, E. Alguire, B. Austin, G. J. O. Beran, Y. A. Bernard, E. Berquist, K. Brandhorst, K. B. Bravaya, S. T. Brown, D. Casanova, C.-M. Chang, Y. Chen, S. H. Chien, K. D. Closser, D. L. Crittenden, M. Diedenhofen, R. A. DiStasio, H. Do, A. D. Dutoi, R. G. Edgar, S. Fatehi, L. Fusti-Molnar, A. Ghysels, A. Golubeva-Zadorozhnaya, J. Gomes, M. W. D. Hanson-Heine, P. H. P. Harbach, A. W. Hauser, E. G. Hohenstein, Z. C. Holden, T.-C. Jagau, H. Ji, B. Kaduk, K. Khistyaev, J. Kim, J. Kim, R. A. King, P. Klunzinger, D. Kosenkov, T. Kowalczyk, C. M. Krauter, K. U. Lao, A. D. Laurent, K. V. Lawler, S. V. Levchenko, C. Y. Lin, F. Liu, E. Livshits, R. C. Lochan, A. Luenser, P. Manohar, S. F. Manzer, S.-P. Mao, N. Mardirossian, A. V. Marenich, S. A. Maurer, N. J. Mayhall, E. Neuscamman, C. M. Oana, R. Olivares-Amaya, D. P. O'Neill, J. A. Parkhill, T. M. Perrine, R. Peverati, A. Prociuk, D. R. Rehn, E. Rosta, N. J. Russ, S. M. Sharada, S. Sharma, D. W. Small, A. Sodt, T. Stein, D. Stück, Y.-C. Su, A. J. W. Thom, T. Tsuchimochi, V. Vanovschi, L. Vogt, O. Vydrov, T. Wang, M. A. Watson, J. Wenzel, A. White, C. F. Williams, J. Yang, S. Yeganeh, S. R. Yost, Z.-Q. You, I. Y. Zhang, X. Zhang, Y. Zhao, B. R. Brooks, G. K. L. Chan, D. M. Chipman, C. J. Cramer, W. A. Goddard, M. S. Gordon, W. J. Hehre, A. Klamt, H. F. Schaefer, M. W. Schmidt, C. D. Sherrill, D. G. Truhlar, A. Warshel, X. Xu, A. Aspuru-Guzik, R. Baer, A. T. Bell, N. A. Besley, J.-D. Chai, A. Dreuw, B. D. Dunietz, T. R. Furlani, S. R. Gwaltney, C.-P. Hsu, Y. Jung, J. Kong, D. S. Lambrecht, W. Liang, C. Ochsenfeld, V. A. Rassolov, L. V. Slipchenko, J. E. Subotnik, T. Van Voorhis, J. M. Herbert, A. I. Krylov, P. M. W. Gill and M. Head-Gordon, *Mol. Phys.*, 2015, **113**, 184-215.
36. Q. Wu and T. Van Voorhis, *Phys. Rev. A*, 2005, **72**, 024502.
37. Y. Zhao and D. G. Truhlar, *Theor. Chem. Acc.*, 2008, **120**, 215-241.
38. Y. Zhao and D. G. Truhlar, *Acc. Chem. Res.*, 2008, **41**, 157-167.
39. Y. Zhao and D. G. Truhlar, *Rev. Mineral. Geochem.*, 2010, **71**, 19-37.
40. D. M. Chipman, *J. Chem. Phys.*, 2000, **112**, 5558-5565.
41. E. Cancès, B. Mennucci and J. Tomasi, *J. Chem. Phys.*, 1997, **107**, 3032-3041.
42. D. Andrae, U. Haussermann, M. Dolg, H. Stoll and H. Preuss, *Theor. Chim. Acta*, 1990, **77**, 123-141.
43. W. J. Here, L. Radom, P. v. R. Schleyer and J. A. Pople, *Ab Initio Molecular Orbital Theory*, Wiley: New York, 1989.
44. S. F. Nelsen, S. C. Blackstock and Y. Kim, *J. Am. Chem. Soc.*, 1987, **109**, 677-682.
45. A. Klimkāns and S. Larsson, *Chem. Phys.*, 1994, **189**, 25-31.
46. D. E. Polyansky, D. Cabelli, J. T. Muckerman, T. Fukushima, K. Tanaka and E. Fujita, *Inorg. Chem.*, 2008, **47**, 3958-3968.
47. P. K. Das, M. V. Encinas, S. Steenken and J. C. Scaiano, *J. Am. Chem. Soc.*, 1981, **103**, 4162-4166.